Electronic Supplementary Information for

Critical impacts of metal cocatalysts on oxidation kinetics and optimal reaction conditions of photocatalytic methane reforming

Hiromasa Sato, [a] Hikaru Saito, [a] Taisuke Higashi [a] and Toshiki Sugimoto [*a, b]

[a] Department of Materials Molecular Science, Institute for Molecular Science, Okazaki, Aichi 444-8585, Japan

[b] Graduate Institute for Advanced Studies (SOKENDAI), Okazaki, Aichi 444-8585, Japan

[*]E-mail: toshiki-sugimoto@ims.ac.jp

Contents:

Supplementary Notes

S1. Experimental

S1-1. Photocatalyst preparation

S1-2. Evaluation of photocatalytic activity

S1-3. Amount of adsorbed water molecules under photocatalytic reaction condition

S1-4. Basic characterization of photocatalyst samples

S2. Kinetic analysis of P_{CH_4} profile of R_{CO_2}

S2-1. Case 1: Derivation of the P_{CH_4} profile of CO_2 formation rate under the situation where density of surface reaction sites is sufficiently high and competitive occupation of reaction sites is negligible

S2-2. Case 2: Derivation of the P_{CH_4} profile of CO_2 formation rate under the situation where density of surface reaction sites is low and competitive occupation of reaction sites is substantial

S3. Derivation of the P_{CH_4} profile of CO_2 formation rate in case where the forward reaction of X_1 is not rate-determining

S4. Discussion on the electron/hole transfer at metal/semiconductor interface

S5. Kinetic analysis of P_{CH_4} profile of $R_{C_2H_6}$

S5-1. Case 1: Derivation of the P_{CH_4} profile of C_2H_6 formation rate under the situation where homocoupling ethane formation reaction is occurred on photocatalyst surfaces

S5-2. Case 2: Derivation of the P_{CH_4} profile of C_2H_6 formation rate under the situation where homocoupling ethane formation reaction is occurred in gas-phase

Supplementary References

Supplementary Notes

S1. Experimental

S1-1. Photocatalyst preparation

Commercial bare β-Ga_2O_3 powder (Kojundo Chemical Lab., purity >99.99%) was employed to prepare Pt- and Pd-loaded samples (Pt/Ga_2O_3, Pd/Ga_2O_3) using an impregnation method[1] as follows. The loading amounts of Pt and Pd were 1 wt% or 0.01 wt%. Initially, H_2PtCl_6•$6H_2O$ (Fujifilm Wako Chemicals, purity >99.9%) or $PdCl_2$ (Kishida Chemical, purity >99%) was dissolved in deionized water. The required amounts of Pt and Pd precursors were 26.5, 0.27, 16.7, and 0.17 mg, respectively, to prepare 1 g of Pt(1wt%)/Ga_2O_3, Pt(0.01wt%)/Ga_2O_3, Pd(1wt%)/ Ga_2O_3, and Pd(0.01wt%)/Ga_2O_3. These aqueous solutions were then added to Ga_2O_3 powder dispersed in deionized water. The slurry was heated to 368 K for 1.5 h using a magnetic stirrer. To evaporate the solvent completely, the obtained powder was dried overnight in an oven at 373 K. Finally, the powder was calcinated for 2 h at 673 K using a muffle furnace.

Before the photocatalytic reaction, the as-prepared Pt- and Pd-loaded Ga_2O_3 photocatalysts were further reduced in H_2 gas using a batch reaction chamber. In this reduction process, the metal loaded photocatalyst samples were heated to 393 K for 3 min using a halogen heater in the chamber filled with 2 kPa of H_2 gas. These reduced photocatalysts were subsequently used for the photocatalytic reaction without exposure to air, as described in the following Supplementary Note S1-2. We confirmed that these reduced Pt and Pd are metallic based on X-ray diffraction (XRD) measurement, and diffuse reflectance infrared Fourier transform (DRIFT) spectroscopy of CO adsorbates sensitive to the oxidation state of surface metal atoms (see Supplementary Note S1-4 for details of the characterizations).[2]

S1-2. Evaluation of photocatalytic activity

The reaction activities of the photocatalysts were evaluated using a batch reaction chamber with a base pressure lower than 1×10^{-3} Pa. The reaction chamber and gas-dosing lines are constructed with stainless-steel ConFlat flanges sealed by metal gaskets and were evacuated to ultra-high vacuum by a turbomolecular pump. Quadrupole mass spectrometer (QMS, QMG220; Pfeiffer Vacuum) operated under ultra-high vacuum conditions confirmed that there is no appreciable leakage of air. The photocatalysts (~2 mg) in the chamber filled with water vapor and methane (CH_4) gas (Sumitomo Seika, purity >99.99%) were irradiated with ultraviolet (UV) light through a CaF_2 window. Water vapor was pre-degassed in an ultra-high vacuum gas line via freeze-pump-thaw cycles of ultrapure water (Fujifilm Wako Chemicals) and introduced into the chamber. The light source was a Xe lamp with high-intensity emission in the deep UV region (UXM-500SX; Ushio), and optical fibers were used to direct the light onto the photocatalysts. The intensity of the light incident on the photocatalysts at a wavelength of 260 ± 15 nm was approximately 90 mW cm^{-2} measured by a UV meter (UVR-300; TOPCON).

The temperatures of the samples were measured using a chromel-alumel thermocouple (type K) and were confirmed to increase from ~295 to ~318 K under UV light irradiation in all photocatalyst samples. It is important to note that experimental conditions (e.g., light intensity, sample temperature) affect reaction activity.[3] For instance, heating the photocatalyst samples leads to the evaporation of adsorbed water molecules, reducing their adsorption amount. Our previous study[4] demonstrated that adsorbed water molecules play a critical role in photocatalytic methane conversion; therefore, modulation of the amount of adsorbed water affects both the activity and selectivity of the photocatalytic process.[5] To ensure the validity and reliability of our experiments, we carefully controlled and standardized these experimental conditions.

The gas in the chamber was sampled every 10 minutes into the analysis chamber, and was analyzed using the well-calibrated QMS. The fragmentation of gaseous molecules was taken into account for the quantification of the gaseous products (See also Supporting Information Section 8 in ref. 2). Note that no appreciable hydrogen evolution and methane conversion occurred without UV irradiation. Furthermore, as reported in detail in Supplementary Note 9 in ref. 4, no appreciable hydrogen evolution and methane conversion occur at 318 K with a halogen heater (typical temperature under photocatalytic reaction condition).

S1-3. Amount of adsorbed water molecules under photocatalytic reaction condition

Using the home-made batch reactor system, the photocatalytic activities were evaluated at several methane pressures (P_{CH_4}) under wet conditions, where the water vapor pressure (P_{H_2O}) was fixed at 2 kPa. At the typical reaction temperature of 318 K, the P_{H_2O} value of 2 kPa corresponds to a relative humidity (RH) of ~20%. As shown in Fig. S1-1 and Supplementary Note 1 in ref. 4, we plotted the amount of adsorbed water as a function of RH. Based on this plot (Fig. S1b), the photocatalyst surfaces are estimated to be covered with one monolayer (1 ML) of adsorbed water molecules under the reaction condition at a relative humidity of ~20%.

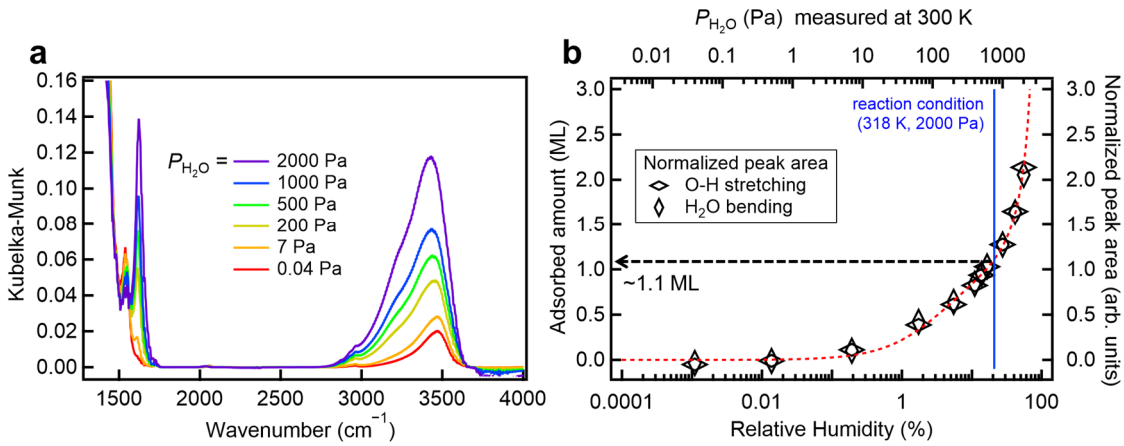

Fig. S1-1. (**a**) Infrared (IR) spectra of water species adsorbed on Pt(1wt%)/Ga_2O_3 photocatalyst surfaces at various water vapor pressures (P_{H_2O}). The background spectrum was obtained using Si powder. (**b**) The measured IR peak areas normalized by the fitting parameter *a* (eq. (*S*1_1) in ref. 4) for both the O–H stretching mode and H–O–H bending mode as a function of relative humidity (RH). The red dotted line shows the RH dependence of the amount of adsorbed water molecules in units of ML (~10^{15} molecules/cm^2) derived from a curve fitting with the Brunauer–Emmett–Teller (BET) adsorption isotherm (eq. (*S*1_1) in ref. 4). The blue vertical line represents the ~20% RH under the practical photocatalytic reaction conditions with UV irradiation (P_{H_2O} = 2 kPa and T = 318 K), indicating that 1.1 ML water molecules are adsorbed on the Pt(1wt%)/Ga_2O_3 samples under the reaction conditions.

S1-4. Basic Characterization of Photocatalyst Samples

• Scanning electron microscopy (SEM)

The SEM images of the as-prepared photocatalysts are shown in Fig. S1-2. The shape of the bare Ga_2O_3 particle was close to a rectangular with sizes of 2–3 μm.[2, 5] After metal loading, no significant changes in macroscopic particle shape were observed, regardless of their loading amount (1wt% or 0.01wt%) and loading metals (Pd: Fig. S1-2 and Pt: Fig. S1-3). Furthermore, the SEM image of the photocatalyst samples remains almost unchanged even after photocatalytic reaction (Fig. S1-3).

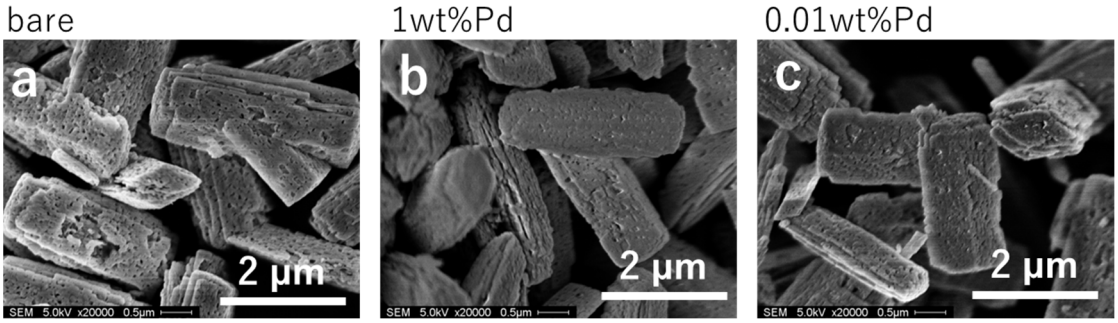

Fig. S1-2. SEM images of the as-prepared (**a**) bare Ga_2O_3, (**b**) Pd(1wt%)/Ga_2O_3, (**c**) Pd(0.01wt%)/Ga_2O_3 photocatalysts before using for reaction.

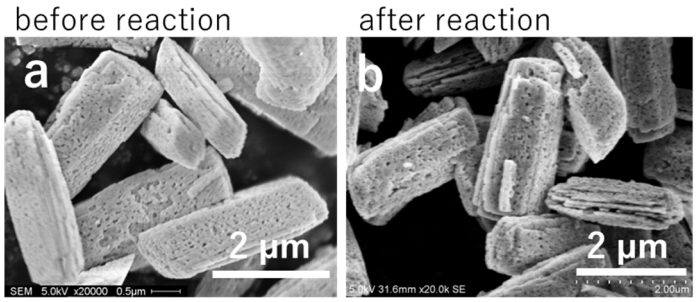

Fig. S1-3. SEM images of the Pt(1wt%)/Ga_2O_3 photocatalysts (**a**) before using for reaction and (**b**) after photocatalytic reaction (P_{CH_4} = 90 kPa, P_{H_2O} = 2 kPa).

• Specific surface area

The amount of adsorbed N_2 was measured at 77 K using a Monosorb MS-21 instrument (Quantachrome), and the specific surface areas were calculated based on the BET theory. The BET surface areas of the bare Ga_2O_3, Pt(1wt%)/Ga_2O_3, Pd(1wt%)/Ga_2O_3, and Pd(0.01wt%)/Ga_2O_3 photocatalysts were 9.8, 9.4, 9.0, and 9.9 m^2/g, respectively.[2] Thus, the surface areas of the photocatalysts remained almost unchanged after metal loading, in good agreement with the SEM images of sample particles (Fig. S1-2, S1-3). These results also indicate that the surface area has little influence on the impact of metal loading on the photocatalytic performance (Fig. 1, 3 in the main text).

• **X-ray diffraction (XRD)**

The crystal structures of bare Ga_2O_3, reduced Pt/Ga_2O_3, and reduced Pd/Ga_2O_3 photocatalysts were measured using XRD (XRD-6000; Shimadzu). The bulk structure of bare Ga_2O_3 particles were in good agreement with the single crystal β- Ga_2O_3 structure (a = 12.23 Å, b = 3.04 Å, c = 5.80 Å),[6] which was maintained after Pt and Pd loading (Fig. S1-4). In addition, a small diffraction peak attributed to Pt(111) was observed at 39.8° in the reduced Pt(1wt%)/Ga_2O_3 photocatalysts,[7] demonstrating the presence of Pt particles on the Ga_2O_3 surface.[2] In contrast, no diffraction peaks derived from Pd species were observed for the Pd(1wt%)/Ga_2O_3 sample, indicating that the Pd nanoparticles were extremely small and highly dispersed on the Ga_2O_3 surface.[2] Note that the presence of Pd on the Ga_2O_3 surface was also confirmed by the following ultraviolet-visible (UV-Vis) spectroscopy measurements (Fig. S1-5), and the Pd cocatalyst was present as nanoparticles rather than atomically dispersed species based on the shape of the IR spectrum of the adsorbed CO species (Fig. S1-6).

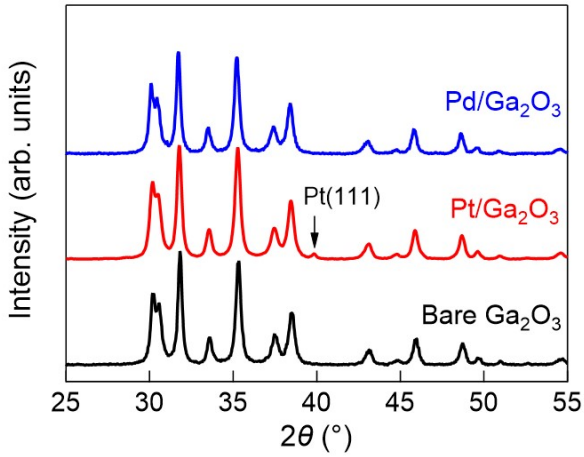

Fig. S1-4. XRD patterns of the bare Ga_2O_3, reduced Pt(1wt%)/Ga_2O_3 and reduced Pd(1wt%)/Ga_2O_3 photocatalysts.

• **Diffuse reflectance ultraviolet-visible (UV-Vis) spectroscopy**

The UV-Vis spectra of the bare Ga_2O_3, as-prepared Pt/Ga_2O_3, and as-prepared Pd/Ga_2O_3 photocatalysts were recorded using a V-670 instrument (JASCO). As shown in Fig. S1-5, the spectrum of the bare Ga_2O_3 exhibited an absorption band below 300 nm, which was attributed to the band gap transition of β-Ga_2O_3 (~4.7 eV). In addition, 1wt% and 0.01wt% of metal loading extended the absorption edge to the visible light region (see also the enlarged inset figure for the as-prepared Pd(0.01wt%)/Ga_2O_3 photocatalysts in Fig. S1-5). These results clearly indicate the presence of Pt and Pd on the Ga_2O_3 surface.[2]

Note that the absorption band at 300–600 nm observed on Pd/Ga_2O_3 would be attributed to charge transfer bands and d–d transitions of Pd^{2+}.[8] Although this indicates that the metal cocatalysts on the as-prepared photocatalysts are oxidized, we confirmed that our reduction treatment fully reduces the cocatalysts based on the following IR spectrum of the adsorbed CO species (Fig. S1-6).

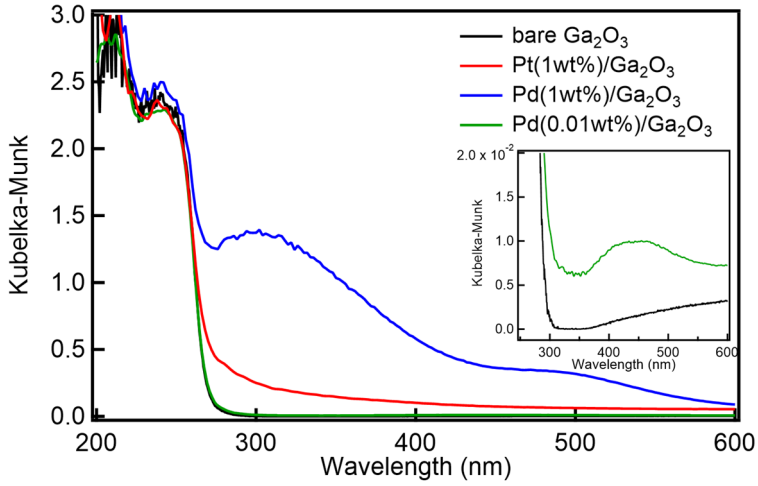

Fig. S1-5. UV-Vis spectra of the bare Ga_2O_3, as-prepared $Pt(1wt\%)/Ga_2O_3$, $Pd(1wt\%)/Ga_2O_3$, and as-prepared $Pd(0.01wt\%)/Ga_2O_3$ photocatalysts. Inset: enlarged figure for the bare and as-prepared $Pd(0.01wt\%)/Ga_2O_3$ photocatalysts.

• IR spectroscopy of adsorbed CO molecules

To confirm the oxidation state of the Pt and Pd cocatalysts after the reduction treatment, IR spectroscopy was conducted under 500 Pa of CO gas in the batch reaction chamber and we observed the stretching frequency of CO adsorbates on the reduced Pt and Pd cocatalysts (Fig. S1-6).[2] The Pt/Ga_2O_3 sample showed C–O stretching peaks at ~2076 cm^{-1} and ~1865 cm^{-1}, corresponding to on-top and bridge sites of metallic Pt.[9, 10] Similarly, Pd/Ga_2O_3 exhibited peaks at ~2100 cm^{-1} and ~1970 cm^{-1}, attributed to on-top and bridge/hollow sites of metallic Pd.[11, 12] Note that adsorbed CO on oxidized Pt (Pt^{2+}) and Pd (Pd^{2+}) sites are known to be observed at ~2100 cm^{-1} for on-top Pt^{2+} sites[13] and ~2140 cm^{-1} for on-top Pd^{2+} sites,[14] respectively. Therefore, the negligibly small intensity of CO adsorbates derived from the oxidized Pt or Pd sites (Fig. S1-6) indicates that both cocatalysts remained in their metallic state after H_2 reduction treatment.

The spectral features of the C–O stretching modes further indicate that the Pt and Pd cocatalysts existed as nanoparticles rather than single atoms. The IR spectra of single metal atoms show sharp and symmetric peaks due to the homogeneous on-top adsorption sites.[15] In contrast, nanoparticles provide a variety of adsorption environments (e.g.,

terrace, step, and edge sites), resulting in broader and more asymmetric spectral features. In our study, the presence of bridge and hollow site adsorption suggests that the Pt and Pd cocatalysts were present as nanoparticles rather than isolated single atoms.[2]

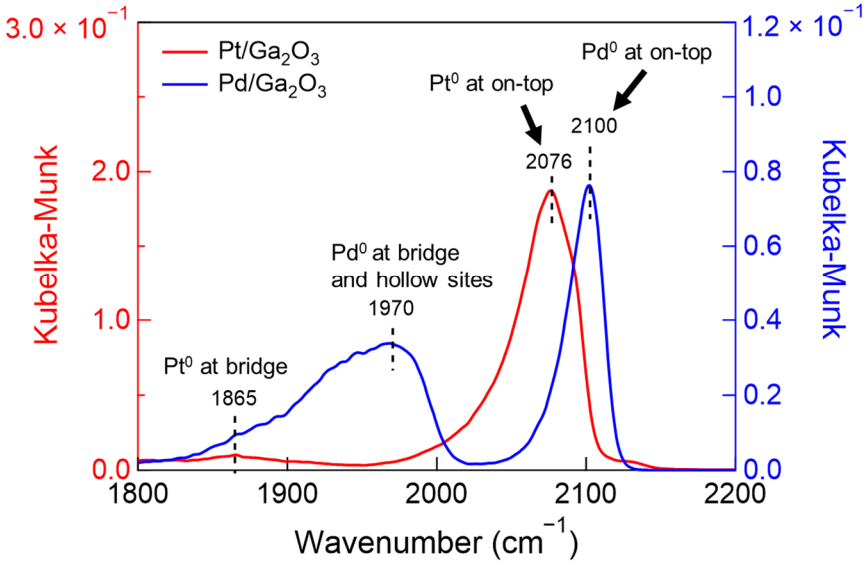

Fig. S1-6. DRIFT spectra of adsorbed CO species (P_{CO} = 500 Pa) on the reduced Pt(1wt%)/Ga_2O_3 and Pd(1wt%)/Ga_2O_3 photocatalysts.

S2. Kinetic analysis of P_{CH_4} profile of R_{CO_2}

As previously reported on the photocatalytic steam reforming of CH_4,[2, 4] the CH_4-transformation process at the photocatalyst surface is divided into three steps, as shown in Fig. S2-1a: i) adsorption and desorption of CH_4 at vacant active sites, ii) sequential reactions of surface intermediate species, and iii) desorption of the final surface products. In the first step, CH_4 undergoes dissociative chemisorption (X_1 = $^{\bullet}CH_3$). The methyl radical X_1 species is further oxidized to form the second intermediate surface species, denoted as X_2 (CH_2 or CH_3OH species in Fig. S2-1b). Our previous study suggested that this reaction involving X_1 ($^{\bullet}CH_3$) intermediate species ($X_1 \rightarrow X_2$) is the rate-determining step.[4] Intermediate species X_2 are further converted to CO_2 (X_8) via multiple intermediate species on the photocatalyst surface and surface-adsorbed CO_2 (X_8) intermediate species finally desorb as a gaseous product (Fig. S2-1a).

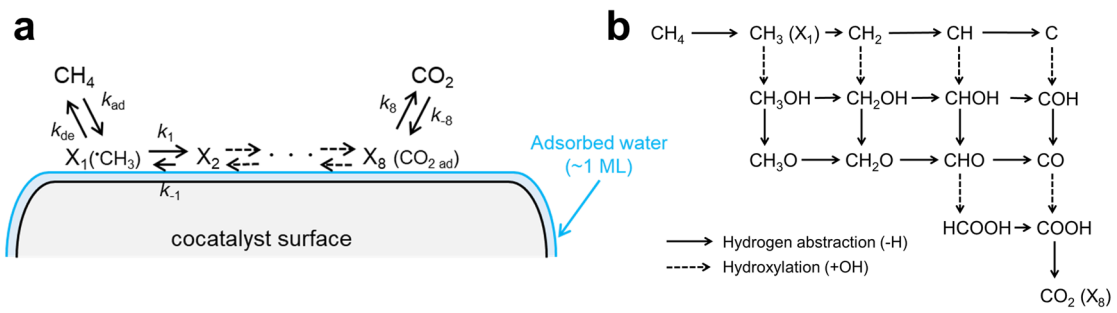

Fig. S2-1. (**a**) Schematic kinetic models of CO_2-formation on photocatalyst surfaces covered with ~1 ML of water molecules. X_i (i = 1, 2, ..., 8) represents i-th reaction intermediates; specifically, X_1 and X_8 denote methyl radical ($^{\bullet}CH_3$) and adsorbed CO_2, respectively. (**b**) Possible reaction pathways from CH_4 to CO_2 in Fig. S2-1a.[16, 17] The number of intermediates in CO_2 formation processes are assumed to be 8 based on the number of holes that are needed to convert CH_4. These oxidation processes are induced through hydrogen abstraction or hydroxylation with preactivated water species such as OH radicals ($^{\bullet}OH$). For simplicity, the contribution of the preactivated water species generated via water oxidation ($H_2O + h^+ \rightarrow {}^{\bullet}OH + H^+$)[4] is omitted in these figures.

The sequential oxidation processes shown in Fig. S2-1 are induced through hydrogen abstraction (R–H + $^{\bullet}$OH → R + H_2O) or hydroxylation (R + $^{\bullet}$OH → ROH) by $^{\bullet}$OH species generated via photocatalytic activation of water ($H_2O + h^+ \rightarrow {}^{\bullet}OH + H^+$). Although the holes get more stabilized through methane oxidation ($CH_4 + h^+ \rightarrow {}^{\bullet}CH_3 + H^+$, 2.06 V vs. SHE)[18] than water oxidation ($H_2O + h^+ \rightarrow {}^{\bullet}OH + H^+$, 2.73 V vs. SHE)[19] from the thermodynamic point of view, the oxidation of water precedes that of methane.[4] This indicates that the photocatalytic oxidation by the surface holes is under kinetic control, rather than thermodynamic control because adsorbed water has higher accessibility to the surface holes than methane in the gas-phase. This feature is also supported by molecular dynamics simulations which revealed that the barrier for water activation is lower than that for methane activation.[4] Based on these findings, we assume that the amount of surface OH radical species are constant and consider the simplified CO_2-formation process ($CH_4 \rightarrow X_1 \rightarrow X_2 \rightarrow \cdots \rightarrow X_8 \rightarrow CO_2$) without explicitly describing the contribution of OH radical species in this section.

In the following two subsections (Supplementary Notes S2-1 and S2-2), we derive the P_{CH_4} profile of the formation rate of CO_2 (R_{CO_2}) under two situations: (Case 1) the density of surface reaction sites is high enough that most of the surface active sites are assumed to be unoccupied and (Case 2) the density of surface reaction sites is not sufficiently high and the variation of the amount of vacant active sites should be explicitly considered, respectively. Since the observed product yields were linearly increased with UV irradiation time,[2, 4] we assumed that the photocatalytic reaction proceeds in the steady-state in the following sections.

S2-1. Case 1: Derivation of the P_{CH_4} profile of CO_2 formation rate under the situation where density of surface reaction sites is sufficiently high and competitive occupation of reaction sites is negligible

In this subsection, the P_{CH_4} profile of R_{CO_2} (Fig. 1a and eq. (3) in the main text) is derived under the condition where the density of surface reaction sites is sufficiently high and most active sites remain unoccupied. Here, we consider a reaction model in which the active sites for each intermediate species (X_1, X_2, …, X_8) are independent. Within this framework, the sites responsible for the dissociative adsorption of methane and the formation of $^{\bullet}CH_3$ (X_1) species ($CH_4 \rightarrow X_1$) are distinct from the sites facilitating their subsequent reaction ($X_1 \rightarrow X_2$). When the forward reaction of the X_1 ($^{\bullet}CH_3$) species is rate-determining,[2, 4] the formed X_2 species are immediately converted to the next intermediate species (X_3), ensuring that the further reaction sites for the X_1 species soon become available. As a result, competitive occupation of reaction sites does not occur, even at high P_{CH_4}, where the adsorption sites for X_1 species are almost fully occupied (Fig. S2-2). Therefore, this reaction model effectively represents the situation where most of the active sites for the rate-determining reaction ($X_1 \rightarrow X_2$) remain unoccupied.

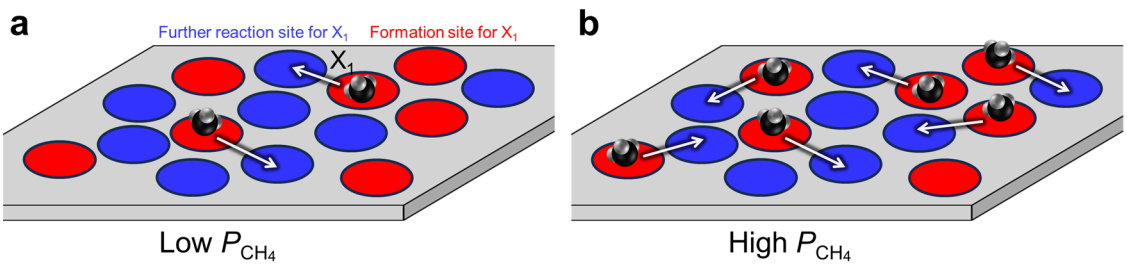

Fig. S2-2. Schematic reaction models for the formation of the rate-determining $^{\bullet}CH_3$ (X_1) intermediate species and further reaction to X_2 species at the next reaction sites under the condition where density of surface reaction sites is sufficiently high and competitive occupation of reaction sites is negligible. Red circles represent the sites for X_1 species formation ($CH_4 \rightarrow X_1$), and blue circles represent the sites for further reaction of X_1 species ($X_1 \rightarrow X_2$). (**a**) Under low P_{CH_4} conditions, the population of $^{\bullet}CH_3$ species increases with P_{CH_4} and the total reaction rate is increased. (**b**) Under high P_{CH_4} conditions, since the adsorption sites of X_1 species (red circles) are almost fully occupied, the total reaction rate is saturated. In this case, competitive occupation of reaction sites is negligible since most of the active sites for the further reaction of X_1 species (blue circles) remain unoccupied.

In this case, multiple reactions involving the intermediates (X_1, X_2, …, X_8) occur on the photocatalyst surface, and the subsequent desorption of the final product molecules is modeled as follows:

$$\mathrm{CH}_{4(\mathrm{gas})} + *_1 \underset{k_{\mathrm{de}}}{\overset{k_{\mathrm{ad}}}{\rightleftarrows}} \mathrm{X}_1, \qquad (S1\_0)$$

$$\mathrm{X}_1 + *_2 \underset{k_{-1}}{\overset{k_1}{\rightleftarrows}} \mathrm{X}_2 + *_1, \qquad (S1\_1)$$

$$\mathrm{X}_2 + *_3 \underset{k_{-2}}{\overset{k_2}{\rightleftarrows}} \mathrm{X}_3 + *_2, \qquad (S1\_2)$$

$$\vdots$$

$$\mathrm{X}_j + *_{j+1} \underset{k_{-j}}{\overset{k_j}{\rightleftarrows}} \mathrm{X}_{j+1} + *_j, \qquad (S1\_j)$$

$$\vdots$$

$$\mathrm{X}_7 + *_8 \underset{k_{-7}}{\overset{k_7}{\rightleftarrows}} \mathrm{X}_8 + *_7, \qquad (S1\_7)$$

$$\mathrm{X}_8 \underset{k_{-8}}{\overset{k_8}{\rightleftarrows}} \mathrm{CO}_{2(\mathrm{gas})} + *_8, \qquad (S1\_8)$$

where the j-th intermediate species is labeled X_j (j = 1 for the methyl radical), the final product molecule (j = 8) is labeled X_8, and $*_j$ denotes the vacant surface sites for the X_j intermediates. The net CH_4-adsorption rate in the initial CH_4 activation process (R_0), net reaction rate of j-th intermediate species (R_j), and net desorption rate of the final product molecule (R_8) are described as follows:

$$R_0 = k_{\mathrm{ad}} P_{\mathrm{CH_4}} N_{\mathrm{v}_1} - k_{\mathrm{de}} N_{\mathrm{X}_1} = k_{\mathrm{ad}} P_{\mathrm{CH_4}} N_{\mathrm{max}_1} \left(\theta_{\mathrm{v}_1} - K_0^{-1} P_{\mathrm{CH_4}}^{-1} \theta_{\mathrm{X}_1}\right), \qquad (S2\_0)$$

$$R_1 = k_1 N_{\mathrm{X}_1} N_{\mathrm{v}_2} - k_{-1} N_{\mathrm{X}_2} N_{\mathrm{v}_1} = k_1 N_{\mathrm{max}_1} N_{\mathrm{max}_2} \left(\theta_{\mathrm{X}_1} \theta_{\mathrm{v}_2} - K_1^{-1} \theta_{\mathrm{X}_2} \theta_{\mathrm{v}_1}\right), \qquad (S2\_1)$$

$$\vdots$$

$$R_j = k_j N_{\mathrm{X}_j} N_{\mathrm{v}_{j+1}} - k_{-j} N_{\mathrm{X}_{j+1}} N_{\mathrm{v}_j} = k_j N_{\mathrm{max}_j} N_{\mathrm{max}_{j+1}} \left(\theta_{\mathrm{X}_j} \theta_{\mathrm{v}_{j+1}} - K_j^{-1} \theta_{\mathrm{X}_{j+1}} \theta_{\mathrm{v}_j}\right), \qquad (S2\_j)$$

$$\vdots$$

$$R_7 = k_7 N_{\mathrm{X}_7} N_{\mathrm{v}_8} - k_{-7} N_{\mathrm{X}_8} N_{\mathrm{v}_7} = k_7 N_{\mathrm{max}_7} N_{\mathrm{max}_8} \left(\theta_{\mathrm{X}_7} \theta_{\mathrm{v}_8} - K_7^{-1} \theta_{\mathrm{X}_8} \theta_{\mathrm{v}_7}\right), \qquad (S2\_7)$$

$$R_8 = k_8 N_{\mathrm{X}_8} - k_{-8} P_{\mathrm{CO_2}} N_{\mathrm{v}_8} = k_8 N_{\mathrm{max}_8} \left(\theta_{\mathrm{X}_8} - K_8^{-1} P_{\mathrm{CO_2}} \theta_{\mathrm{v}_8}\right), \qquad (S2\_8)$$

where K_j denotes the equilibrium constant of the j-th reaction ($K_j \equiv k_j/k_{-j}$). N_{X_j} and N_{v_j} are the number of filled and vacant surface sites for j-th intermediate species (X_j), respectively. θ_{X_j} ($\equiv N_{\mathrm{X}_j}/N_{\mathrm{max}_j}$) and θ_{v_j} ($\equiv N_{\mathrm{v}_j}/N_{\mathrm{max}_j}$) are the coverage and the fraction of vacant surface sites for X_j, respectively. N_{max_j} is the sum of the numbers of filled and vacant surface sites for X_j species ($N_{\mathrm{max}_j} = N_{\mathrm{X}_j} + N_{\mathrm{v}_j} \Leftrightarrow 1 = \theta_{\mathrm{X}_j} + \theta_{\mathrm{v}_j}$). Using these net reaction rates (R_j), the following rate equations are obtained:

$$\frac{\mathrm{d}N_{\mathrm{X}_1}}{\mathrm{d}t} = R_0 - R_1, \qquad (S3\_0)$$

$$\frac{\mathrm{d}N_{\mathrm{X}_2}}{\mathrm{d}t} = R_1 - R_2, \qquad (S3\_1)$$

$$\vdots$$

$$\frac{\mathrm{d}N_{\mathrm{X}_j}}{\mathrm{d}t} = R_{j-1} - R_j, \qquad (S3\_j-1)$$

$$\frac{\mathrm{d}N_{\mathrm{X}_{j+1}}}{\mathrm{d}t} = R_j - R_{j+1}, \qquad (S3\_j)$$

$$\vdots$$

$$\frac{\mathrm{d}N_{\mathrm{X}_8}}{\mathrm{d}t} = R_7 - R_8, \qquad (S3\_7)$$

$$\frac{\mathrm{d}N_{\mathrm{CO}_2(\mathrm{gas})}}{\mathrm{d}t} = R_8, \qquad (S3\_8)$$

where $N_{\mathrm{CO_2(gas)}}$ is the number of produced CO_2 gas molecules, whose time derivative ($\mathrm{d}N_{\mathrm{CO_2(gas)}}/\mathrm{d}t$) represent the CO_2 formation rate, $R_{\mathrm{CO_2}}$.

Under steady-state reaction conditions, the density of X_j is constant ($\mathrm{d}N_{X_j}/\mathrm{d}t \approx 0 \Leftrightarrow R_{j-1} \approx R_j$). As a result, the formation rate of CO_2 can be expressed as follows:

$$R_{\mathrm{CO_2}} \equiv R_8 \approx R_7 \approx \cdots \approx R_2 \approx R_1 \approx R_0. \qquad (S4)$$

In particular, when the forward reaction of the $^{\bullet}CH_3$ (= X_1) species (eq. ($S1\_1$)) is rate-determining,[2, 4] the relation $\theta_{X_1} >> \theta_{X_2}$ is satisfied and the following equation is obtained from eqs. ($S2\_1$) and ($S4$):

$$R_{\mathrm{CO_2}} \approx R_1 = k_1 N_{\mathrm{max}_1} N_{\mathrm{max}_2}\left(\theta_{\mathrm{X}_1}\theta_{\mathrm{v}_2} - K_1^{-1}\theta_{\mathrm{X}_2}\theta_{\mathrm{v}_1}\right) \approx k_1 N_{\mathrm{max}_1} N_{\mathrm{max}_2}\theta_{\mathrm{X}_1}\theta_{\mathrm{v}_2}. \qquad (S5)$$

Defining the rate constant factor k_1' as $k_1' \equiv k_1 N_{\mathrm{max}_1} N_{\mathrm{max}_2}$, eq. (2) in the main text is derived:

$$R_{\mathrm{CO_2}} \approx k_1'\theta_{\mathrm{X}_1}\theta_{\mathrm{v}_2}. \qquad (S6)$$

Then, to derive the P_{CH_4} profile of R_{CO_2}, we first focus on the P_{CH_4} profile of θ_{X_1} (= θ_{CH_3}). Since the adsorption and desorption of CH_4 is not the rate-determining step,[4] the relation $k_{ad}P_{CH_4}N_{max_1} >> R_1$ is satisfied. Then, on the basis of the relationships $k_{ad}P_{CH_4}N_{max_1} >> R_1 = R_0$ (see also eq. ($S4$)) and eq. ($S2\_0$), θ_{X_1} is expressed by θ_{v_1} as follows:

$$R_0/\left(k_{\mathrm{ad}}P_{\mathrm{CH_4}}N_{\mathrm{max}_1}\right) = \theta_{\mathrm{v}_1} - K_0^{-1}P_{\mathrm{CH_4}}^{-1}\theta_{\mathrm{X}_1} \ll 1, \qquad (S7)$$

$$\theta_{\mathrm{X}_1} \approx K_0 P_{\mathrm{CH_4}}\theta_{\mathrm{v}_1}. \qquad (S8)$$

Since the total number of surface sites (sum of the vacant and filled sites) of the X_1 species is constant,

$$1 = \theta_{\mathrm{v}_1} + \theta_{\mathrm{X}_1}. \qquad (S9)$$

From eqs. (*S*8) and (*S*9), eq. (1) in the main text (Langmuir-adsorption-isotherm type equation) is derived as

$$\theta_{\mathrm{CH_3}} \equiv \theta_{\mathrm{X_1}} \approx \frac{K_0 P_{\mathrm{CH_4}}}{1 + K_0 P_{\mathrm{CH_4}}}. \qquad (S10)$$

The adsorption-desorption equilibrium constant $K_0 \equiv k_{\mathrm{ad}}/k_{\mathrm{de}}$, a key parameter for the dependence of $P_{\mathrm{CH_4}}$, is given by

$$k_{\mathrm{ad}} = \frac{sA}{\sqrt{2\pi M k_{\mathrm{B}} T_{\mathrm{g}}}} \exp\left(-\frac{E_{\mathrm{ad}}}{k_{\mathrm{B}} T_{\mathrm{s}}}\right), \qquad (S11)$$

$$k_{\mathrm{de}} = \nu_0 \exp\left(-\frac{E_{\mathrm{de}}}{k_{\mathrm{B}} T_{\mathrm{s}}}\right), \qquad (S12)$$

$$K_0 = \frac{sA}{\nu_0\sqrt{2\pi M k_{\mathrm{B}} T_{\mathrm{g}}}} \exp\left(\frac{E_{\mathrm{de}} - E_{\mathrm{ad}}}{k_{\mathrm{B}} T_{\mathrm{s}}}\right) \equiv \frac{sA}{\nu_0\sqrt{2\pi M k_{\mathrm{B}} T_{\mathrm{g}}}} \exp\left(\frac{U}{k_{\mathrm{B}} T_{\mathrm{s}}}\right), \qquad (S13)$$

where M is the mass of a CH_4 molecule (2.66×10^{-26} kg), k_B is the Boltzmann constant (1.38×10^{-23} J/K), T_g is the temperature of gaseous CH_4 (~296 K), T_s is the temperature of the photocatalyst surface (~318 K), ν_0 is the frequency factor[20] (1.0×10^{13} s^{-1}), s is the sticking coefficient of CH_4, A is the area occupied by adsorbed CH_4 (1.0×10^{-15} cm^2), E_{ad} is the activation energy of dissociative adsorption of CH_4, E_{de} is the activation energy of desorption of CH_4, and U ($\equiv E_{de}-E_{ad}$) represents the stabilization energy of the adsorbed methyl radicals. The P_{CH_4} profiles of θ_{X_1} ($= \theta_{CH_3}$) at typical values of U are displayed in Fig. 2c in the main text. As U increases, the coverage starts increasing at the lower P_{CH_4}. With increasing P_{CH_4}, the coverage monotonically increases as an upward convex curve and then saturates (Fig. 2c).

Then, to fully derive the P_{CH_4} profile of R_{CO_2}, we next focus on θ_{v_2} (see eq. (*S*6)). In the case where competitive occupation is negligible (Fig. S2-2), most of the active sites for the further reaction of X_1 species remain unoccupied ($\theta_{v_2} \approx 1$). This situation is substantial when the reaction step of X_1 ($X_1 \rightarrow X_2$) is rate-determining[2, 4] and the formed X_2 species are immediately converted to the next intermediate species ($\theta_{X_2} \approx 0$). Therefore, the P_{CH_4} profile of R_{CO_2} (eq. (3) in the main text) is derived from eqs. (*S*6) and (*S*10) as

$$R_{\mathrm{CO_2}} \approx k_1' \theta_{\mathrm{X_1}} \theta_{\mathrm{v_2}} \approx k_1' \left[\frac{K_0 P_{\mathrm{CH_4}}}{1 + K_0 P_{\mathrm{CH_4}}}\right]. \qquad (S14)$$

The maximum R_{CO_2} value of k_1' is given at $\theta_{X_1} = 1$. Since CO_2 formation ($CH_4 + 2H_2O \rightarrow CO_2 + 4H_2$) was the major reaction, the relationship $R_{H_2} \approx 4R_{CO_2}$ was approximately satisfied (Fig. 1a).[4, 21] Therefore, the P_{CH_4} profile of the H_2-formation rate is also described as

$$R_{\mathrm{H_2}} \approx 4R_{\mathrm{CO_2}} \approx 4k_1' \left[\frac{K_0 P_{\mathrm{CH_4}}}{1 + K_0 P_{\mathrm{CH_4}}}\right]. \qquad (S15)$$

S2-2. Case 2: Derivation of the P_{CH_4} profile of CO_2 formation rate under the situation where density of surface reaction sites is low and competitive occupation of reaction sites is substantial

In this subsection, the P_{CH_4} profile of R_{CO_2} (Fig. 1b and eq. (4) in the main text) is derived under the condition where the density of surface reaction sites is not sufficiently high and the variation of the density of vacant active sites should be explicitly considered ($\theta_v \neq 1$). Here, we consider a reaction model in which the active sites are competitively shared among intermediate species (X_1, X_2, …, X_8). Within this framework, the sites responsible for the rate-determining reaction ($X_1 \rightarrow X_2$) are also occupied by the adsorbed $^{\bullet}CH_3$ (X_1) species, resulting in competitive site occupation (Fig. S2-3).

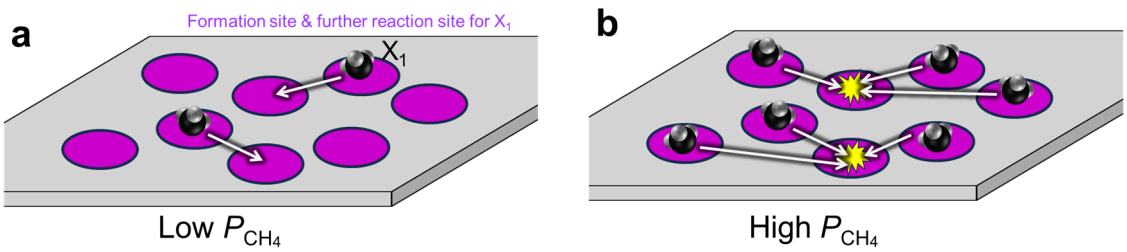

Fig. S2-3. Schematic reaction models for the formation of the rate-determining $^{\bullet}CH_3$ (X_1) intermediate species and further reaction to X_2 species at the next reaction sites under the condition where density of surface reaction sites is low and competitive occupation of reaction sites is substantial. Purple circles represent the surface active sites, on which both formation ($CH_4 \rightarrow X_1$) and further reaction ($X_1 \rightarrow X_2$) of X_1 species are occurred. (**a**) Under low P_{CH_4} conditions, the population of $^{\bullet}CH_3$ species and the total reaction rate increase with P_{CH_4}. (**b**) Under high P_{CH_4} conditions, occupation of surface sites by X_1 species competitively decreases the fraction of vacant sites necessary for the further reaction of X_1 species and induce molecular-level congestion of intermediate species, resulting in the negative effect on the total reaction rate.

Then, multiple reactions involving the intermediates (X_1, X_2, …, X_8) and the subsequent desorption of the final product molecules are modeled as follows:

$$\mathrm{CH_{4(gas)}} + *_{\mathrm{all}} \underset{k_{\mathrm{de}}}{\overset{k_{\mathrm{ad}}}{\rightleftarrows}} \mathrm{X_1}, \qquad (S16\_0)$$

$$\mathrm{X_1} + *_{\mathrm{all}} \underset{k_{-1}}{\overset{k_1}{\rightleftarrows}} \mathrm{X_2} + *_{\mathrm{all}}, \qquad (S16\_1)$$

$$\mathrm{X_2} + *_{\mathrm{all}} \underset{k_{-2}}{\overset{k_2}{\rightleftarrows}} \mathrm{X_3} + *_{\mathrm{all}}, \qquad (S16\_2)$$

$$\vdots$$

$$\mathrm{X}_j + *_{\mathrm{all}} \underset{k_{-j}}{\overset{k_j}{\rightleftarrows}} \mathrm{X}_{j+1} + *_{\mathrm{all}}, \qquad (S16\_j)$$

$$\vdots$$

$$\mathrm{X_7} + *_{\mathrm{all}} \underset{k_{-7}}{\overset{k_7}{\rightleftarrows}} \mathrm{X_8} + *_{\mathrm{all}}, \qquad (S16\_7)$$

$$\mathrm{X_8} \underset{k_{-8}}{\overset{k_8}{\rightleftarrows}} \mathrm{CO_{2(gas)}} + *_{\mathrm{all}}, \qquad (S16\_8)$$

where the j-th intermediate species is labeled X_j (j = 1, $^{\bullet}CH_3$), the final product molecule (j = 8, CO_2) is labeled X_8, and $*_{all}$ denotes the vacant surface active sites available for all intermediates (Fig. S2-3). Note that the vacant sites in this model are given as $*_{all}$ instead of $*_j$ because the active sites are shared among all intermediate species. The net CH_4-adsorption rate in the initial CH_4 activation process (R_0), net reaction rate of j-th intermediate species (R_j), and net desorption rate of the final product molecule (R_8) are described as follows:

$$R_0 = k_{\mathrm{ad}} P_{\mathrm{CH_4}} N_{\mathrm{v_{all}}} - k_{\mathrm{de}} N_{\mathrm{X_1}} = k_{\mathrm{ad}} P_{\mathrm{CH_4}} N_{\mathrm{max_{all}}} \left(\theta_{\mathrm{v_{all}}} - K_0^{-1} P_{\mathrm{CH_4}}^{-1} \theta_{\mathrm{X_1}}\right), \qquad (S17\_0)$$

$$R_1 = k_1 N_{\mathrm{X_1}} N_{\mathrm{v_{all}}} - k_{-1} N_{\mathrm{X_2}} N_{\mathrm{v_{all}}} = k_1 N_{\mathrm{max_{all}}}{}^2 \theta_{\mathrm{v_{all}}} \left(\theta_{\mathrm{X_1}} - K_1^{-1} \theta_{\mathrm{X_2}}\right), \qquad (S17\_1)$$

$$\vdots$$

$$R_j = k_j N_{\mathrm{X}_j} N_{\mathrm{v_{all}}} - k_{-j} N_{\mathrm{X}_{j+1}} N_{\mathrm{v_{all}}} = k_j N_{\mathrm{max_{all}}}{}^2 \theta_{\mathrm{v_{all}}} \left(\theta_{\mathrm{X}_j} - K_j^{-1} \theta_{\mathrm{X}_{j+1}}\right), \qquad (S17\_j)$$

$$\vdots$$

$$R_7 = k_7 N_{\mathrm{X_7}} N_{\mathrm{v_{all}}} - k_{-7} N_{\mathrm{X_8}} N_{\mathrm{v_{all}}} = k_7 N_{\mathrm{max_{all}}}{}^2 \theta_{\mathrm{v_{all}}} \left(\theta_{\mathrm{X_7}} - K_7^{-1} \theta_{\mathrm{X_8}}\right), \qquad (S17\_7)$$

$$R_8 = k_8 N_{\mathrm{X_8}} - k_{-8} P_{\mathrm{CO_2}} N_{\mathrm{v_{all}}} = k_8 N_{\mathrm{max_{all}}} \left(\theta_{\mathrm{X_8}} - K_8^{-1} P_{\mathrm{CO_2}} \theta_{\mathrm{v_{all}}}\right), \qquad (S17\_8)$$

where K_j denotes the equilibrium constant of the j-th reaction ($K_j \equiv k_j/k_{-j}$). N_{X_j} and $N_{v_{all}}$ are the number of filled surface sites for j-th intermediate species (X_j) and vacant surface sites, respectively. θ_{X_j} ($\equiv N_{X_j}/N_{max_{all}}$) and $\theta_{v_{all}}$ ($\equiv N_{v_{all}}/N_{max_{all}}$) are the coverage for X_j and the fraction of vacant surface sites, respectively. $N_{max_{all}}$ is the sum of the numbers of filled

and vacant surface sites ($N_{\max_{\mathrm{all}}} = \Sigma N_{\mathrm{X}_j} + N_{\mathrm{v}_{\mathrm{all}}} \Leftrightarrow 1 = \Sigma\theta_{\mathrm{X}_j} + \theta_{\mathrm{v}_{\mathrm{all}}}$). Using these net reaction rates (R_j), the following rate equations are obtained:

$$\frac{\mathrm{d}N_{\mathrm{X}_1}}{\mathrm{d}t} = R_0 - R_1, \qquad (S18\_0)$$

$$\frac{\mathrm{d}N_{\mathrm{X}_2}}{\mathrm{d}t} = R_1 - R_2, \qquad (S18\_1)$$

$$\vdots$$

$$\frac{\mathrm{d}N_{\mathrm{X}_j}}{\mathrm{d}t} = R_{j-1} - R_j, \qquad (S18\_j-1)$$

$$\frac{\mathrm{d}N_{\mathrm{X}_{j+1}}}{\mathrm{d}t} = R_j - R_{j+1}, \qquad (S18\_j)$$

$$\vdots$$

$$\frac{\mathrm{d}N_{\mathrm{X}_8}}{\mathrm{d}t} = R_7 - R_8, \qquad (S18\_7)$$

$$\frac{\mathrm{d}N_{\mathrm{CO}_{2(\mathrm{gas})}}}{\mathrm{d}t} = R_8, \qquad (S18\_8)$$

Under steady-state reaction conditions, the density of X_j is constant ($\mathrm{d}N_{\mathrm{X}_j}/\mathrm{d}t \approx 0 \Leftrightarrow R_{j-1} \approx R_j$). As a result, the formation rate of CO_2 can be expressed as follows:

$$R_{\mathrm{CO}_2} \equiv R_8 \approx R_7 \approx \cdots \approx R_2 \approx R_1 \approx R_0. \qquad (S19)$$

In particular, when the forward reaction of the $^{\bullet}CH_3$ (= X_1) species (eq. (S16_1)) is rate-determining,[2, 4] the relation $\theta_{\mathrm{X}_1} >> \theta_{\mathrm{X}_2}$ is satisfied and the following equation is obtained from eqs. (S17_1) and (S19):

$$R_{\mathrm{CO}_2} \approx R_1 = k_1 {N_{\max_{\mathrm{all}}}}^2 \theta_{\mathrm{v}_{\mathrm{all}}} \left(\theta_{\mathrm{X}_1} - K_1^{-1}\theta_{\mathrm{X}_2}\right) \approx k_1 {N_{\max_{\mathrm{all}}}}^2 \theta_{\mathrm{X}_1}\theta_{\mathrm{v}_{\mathrm{all}}}. \qquad (S20)$$

Defining the rate constant factor k_1' as $k_1' \equiv k_1 {N_{\max_{\mathrm{all}}}}^2$, eq. (2) in the main text is derived as

$$R_{\mathrm{CO}_2} \approx k_1'\theta_{\mathrm{X}_1}\theta_{\mathrm{v}_{\mathrm{all}}}. \qquad (S21)$$

Then, to derive the P_{CH_4} profile of R_{CO_2}, we first focus on the P_{CH_4} profile of θ_{X_1} (= θ_{CH_3}).[4] Since the adsorption and desorption of CH_4 is not the rate-determining step, the relation $k_{\mathrm{ad}}P_{CH_4}N_{\max_{\mathrm{all}}} >> R_1$ is satisfied. Then, on the basis of the relationships $k_{\mathrm{ad}}P_{CH_4}N_{\max_{\mathrm{all}}} >> R_1 = R_0$ (see also eq. (S19)) and eq. (S17_0), θ_{X_1} is expressed by $\theta_{\mathrm{v}_{\mathrm{all}}}$ as follows:

$$R_0/\left(k_{\mathrm{ad}}P_{\mathrm{CH}_4}N_{\max_{\mathrm{all}}}\right) = \theta_{\mathrm{v}_{\mathrm{all}}} - K_0^{-1}P_{\mathrm{CH}_4}^{-1}\theta_{\mathrm{X}_1} \ll 1, \qquad (S22)$$

$$\theta_{\mathrm{X}_1} \approx K_0 P_{\mathrm{CH}_4}\theta_{\mathrm{v}_{\mathrm{all}}}. \qquad (S23)$$

Since the majority of the surface intermediates are $^{\bullet}CH_3$ (X_1) in case the reaction of adsorbed $^{\bullet}CH_3$ is rate-determining ($\theta_{\mathrm{X}_1} >> \theta_{\mathrm{X}_j}$),[2, 4] the relation $1 = \Sigma\theta_{\mathrm{X}_j} + \theta_{\mathrm{v}_{\mathrm{all}}}$ is approximated as

$$1 \approx \theta_{\mathrm{X}_1} + \theta_{\mathrm{v}_{\mathrm{all}}}, \qquad (S24)$$

which corresponds to the schematics shown in Fig. S2-3. From eqs. ($S23$) and ($S24$), eq. (1) in the main text (Langmuir-adsorption-isotherm type equation) is derived as

$$\theta_{\mathrm{CH_3}} \equiv \theta_{\mathrm{X_1}} \approx \frac{K_0 P_{\mathrm{CH_4}}}{1 + K_0 P_{\mathrm{CH_4}}}. \qquad (S25)$$

Then, to fully derive the $P_{\mathrm{CH_4}}$ profile of $R_{\mathrm{CO_2}}$, we next focus on $\theta_{\mathrm{v_{all}}}$ (see eq. ($S21$)). In the case where the competitive occupation is substantial and the density of active sites is not sufficiently high (Fig. S2-3), the coverage of the rate-determining $\mathrm{X_1}$ intermediate species explicitly affects the fraction of vacant surface sites ($\theta_{\mathrm{v_{all}}} \approx 1 - \theta_{\mathrm{X_1}}$). Therefore, the $P_{\mathrm{CH_4}}$ profile of $R_{\mathrm{CO_2}}$ (eq. (4) in the main text) is derived from eqs. ($S21$) and ($S25$) as

$$R_{\mathrm{CO_2}} \approx k_1' \theta_{\mathrm{X_1}} \theta_{\mathrm{v_{all}}} \approx k_1' \theta_{\mathrm{X_1}} \left(1 - \theta_{\mathrm{X_1}}\right) = k_1' \left[\frac{K_0 P_{\mathrm{CH_4}}}{\left(1 + K_0 P_{\mathrm{CH_4}}\right)^2}\right]. \qquad (S26)$$

Since CO_2 formation ($CH_4 + 2H_2O \rightarrow CO_2 + 4H_2$) was the major reaction, the relationship $R_{\mathrm{H_2}} \approx 4R_{\mathrm{CO_2}}$ was approximately satisfied (Fig. 1b).[4, 21] Therefore, the $P_{\mathrm{CH_4}}$ profile of the H_2-formation rate is also described as

$$R_{\mathrm{H_2}} \approx 4R_{\mathrm{CO_2}} \approx 4k_1' \left[\frac{K_0 P_{\mathrm{CH_4}}}{\left(1 + K_0 P_{\mathrm{CH_4}}\right)^2}\right]. \qquad (S27)$$

Finally, it should be noted that competitive occupation of active sites negatively impacts the maximum $R_{\mathrm{CO_2}}$ value. Specifically, the maximum $R_{\mathrm{CO_2}}$ value is given as $k_1'/4$ at $\theta_{\mathrm{X_1}} = \theta_{\mathrm{v_{all}}} = 1/2$ (eq. ($S26$)). In contrast, when the competitive occupation is negligible (see Supplementary Note S2-1, Case 1), the maximum $R_{\mathrm{CO_2}}$ value reaches k_1' at $\theta_{\mathrm{X_1}} = 1$ (eq. ($S14$)). Consequently, the maximum $R_{\mathrm{CO_2}}$ value without competitive occupation is apparently four times larger than that with competitive occupation. Indeed, as shown in Fig. 1, the maximum $R_{\mathrm{CO_2}}$ value for Pt(1wt%)/Ga_2O_3 samples (~3.0 mmol/h·g) with negligible competitive occupation was approximately four times larger than that for Pt(0.01wt%)/Ga_2O_3 samples (~0.73 mmol/h·g) with substantial competitive occupation. However, Pd(1wt%)/Ga_2O_3 samples (~0.25 mmol/h·g) with negligible competitive occupation exhibited much lower values compared to Pd(0.01wt%)/Ga_2O_3 samples (~1.7 mmol/h·g) with substantial competitive occupation. The rate constant factor k_1' under competitive and non-competitive conditions is defined as $k_1 N_{\mathrm{max_1}} N_{\mathrm{max_2}}$ and $k_1 N_{\mathrm{max_{all}}}^2$, respectively. Thus, the observed increase of approximately one order of magnitude of methane conversion rate when Pd loading is reduced from 1wt% to 0.01wt% suggests a significant enhancement in the turnover frequency of methane oxidation (k_1) or the number of total active sites ($N_{\mathrm{max_{all}}}$). Simply considering that $N_{\mathrm{max_{all}}}$ is expected to decrease

due to the reduced Pd loading, k_1 must have drastically increased more than compensating for the decrease in $N_{\max_{all}}$. While understanding this phenomenon lies beyond the scope of this study, future investigations addressing this issue would provide more valuable insights into improving photocatalytic performance from the perspective of metal-cocatalyst engineering.

S3. Derivation of the P_{CH_4} profile of CO_2 formation rate in case where the forward reaction of X_1 is not rate-determining

In the above discussion, we assumed that the forward reaction of $^{\bullet}CH_3$ (= X_1) species is rate-determining. On the other hand, it is noteworthy to discuss the case where the rate-determining step for the formation of CO_2 is not the surface reaction of X_1, but the surface reaction of the i-th ($i \neq 1$) intermediate species (X_i). In this section, we show that the P_{CH_4} profiles similar to eqs. (3) and (4) in the main text are also derived in this case.

First, we consider the case where density of surface reaction sites is sufficiently high and competitive occupation of reaction sites is negligible (Case 1 in Supplementary Note S2-1). In this case, the active sites for each intermediate species are independent (Fig. S2-2). As discussed in detail in Supplementary Note 6-2 in ref. 4, almost the same P_{CH_4} profile for the formation rates of CO_2 and H_2 (equations similar to eq. (3): Langmuir-adsorption-isotherm type equation) can be expressed in case the reaction of the i-th ($i \neq 1$) intermediate species is the rate-determining step.

$$R_{CO_2} \approx k_i N_{\max_i} N_{\max_{i+1}} \theta_{X_i} = k_i N_{\max_i} N_{\max_{i+1}} \left(\frac{K' P_{CH_4}}{1 + K' P_{CH_4}} \right), \qquad (S28)$$

$$K' \equiv \prod_{f=0}^{i-1} K_f = K_0 K_1 K_2 \cdots K_{i-1}, \qquad (S29)$$

$$R_{H_2} \approx 4 R_{CO_2} \approx 4 k_i N_{\max_i} N_{\max_{i+1}} \left(\frac{K' P_{CH_4}}{1 + K' P_{CH_4}} \right), \qquad (S30)$$

where K' reflects the stabilization energy of the rate-determining i-th intermediate species.[4] In the main text, K_0 and K' were not distinguished and were represented as K for simplicity.

Then, we consider the case where density of surface reaction sites is low and competitive occupation of reaction sites is substantial (Case 2 in Supplementary Note S2-2). In this case, active sites are competitively shared among intermediate species (Fig. S2-3). To derive the P_{CH_4} profile for the formation rate of CO_2 in the case where the surface reaction of the i-th ($i \neq 1$) intermediate species is the rate-determining step, we reconsider the kinetic analysis discussed in Supplementary Note S2-2. As discussed above, the net CH_4-adsorption rate in the initial CH_4 activation process (R_0), net reaction rate of rate-determining i-th intermediate species (R_i), net reaction rate of j-th intermediate species (R_j), and net desorption rate of the final product molecule (R_8) are described as follows (see eq. (S17)):

$$R_0 = k_{ad} P_{CH_4} N_{\max_{all}} \left(\theta_{v_{all}} - K_0^{-1} P_{CH_4}^{-1} \theta_{X_1} \right), \qquad (S31\_0)$$

$$R_i = k_i {N_{\max_{all}}}^2 \theta_{v_{all}} \left(\theta_{X_i} - K_i^{-1} \theta_{X_{i+1}} \right), \qquad (S31\_i)$$

$$R_j = k_j {N_{\max_{\mathrm{all}}}}^2 \theta_{\mathrm{v_{all}}} \left(\theta_{\mathrm{X}_j} - K_j^{-1} \theta_{\mathrm{X}_{j+1}}\right), \qquad (S31\_j)$$

$$R_8 = k_8 N_{\max_{\mathrm{all}}} \left(\theta_{\mathrm{X}_8} - K_8^{-1} P_{\mathrm{CO_2}} \theta_{\mathrm{v_{all}}}\right). \qquad (S31\_8)$$

When the reaction of the i-th ($i \neq 1$) intermediate species (X_i) is the rate-determining step, the relation $\theta_{\mathrm{X}_i} >> \theta_{\mathrm{X}_{i+1}}$ is satisfied and the following equation is obtained from eqs. ($S31\_i$) and ($S19$: $R_{\mathrm{CO_2}} \equiv R_8 \approx \ldots \approx R_i \approx \ldots \approx R_0$):

$$R_{\mathrm{CO_2}} \approx R_i = k_i {N_{\max_{\mathrm{all}}}}^2 \theta_{\mathrm{v_{all}}} \left(\theta_{\mathrm{X}_i} - K_i^{-1} \theta_{\mathrm{X}_{i+1}}\right) \approx k_i {N_{\max_{\mathrm{all}}}}^2 \theta_{\mathrm{X}_i} \theta_{\mathrm{v_{all}}}. \qquad (S32)$$

Here, we derive θ_{X_i} and $\theta_{\mathrm{v_{all}}}$ to derive the $P_{\mathrm{CH_4}}$ profile of $R_{\mathrm{CO_2}}$. In case the reaction of the i-th ($i \neq 1$) intermediate species is the rate-determining step, the relations $k_{\mathrm{ad}} P_{\mathrm{CH_4}} N_{\max_{\mathrm{all}}} >> R_i$, $k_j {N_{\max_{\mathrm{all}}}}^2 >> R_i$ ($1 \leq j \leq 7, j \neq i$), and $k_8 N_{\max_{\mathrm{all}}} >> R_i$ are satisfied. Because of the relationships $k_{\mathrm{ad}} P_{\mathrm{CH_4}} N_{\max_{\mathrm{all}}} >> R_i = R_0$, $k_j {N_{\max_{\mathrm{all}}}}^2 >> R_i = R_j$, and $k_8 N_{\max_{\mathrm{all}}} >> R_i = R_8$ (see also eq. ($S19$)), θ_{X_1} and θ_{X_8} are expressed by $\theta_{\mathrm{v_{all}}}$ and the relationship between the θ_{X_j} and $\theta_{\mathrm{X}_{j+1}}$ is obtained as follows:

$$R_0 / \left(k_{\mathrm{ad}} P_{\mathrm{CH_4}} N_{\max_{\mathrm{all}}}\right) = \theta_{\mathrm{v_{all}}} - K_0^{-1} P_{\mathrm{CH_4}}^{-1} \theta_{\mathrm{X}_1} \ll 1, \qquad (S33)$$

$$\theta_{\mathrm{X}_1} \approx \theta_{\mathrm{v_{all}}} P_{\mathrm{CH_4}} K_0. \qquad (S34)$$

$$R_j / \left(k_j {N_{\max_{\mathrm{all}}}}^2\right) = \theta_{\mathrm{v_{all}}} \left(\theta_{\mathrm{X}_j} - K_j^{-1} \theta_{\mathrm{X}_{j+1}}\right) \ll 1, \qquad (1 \leq j \leq 7, j \neq i) \qquad (S35)$$

$$\theta_{\mathrm{X}_{j+1}} \approx K_j \theta_{\mathrm{X}_j}. \quad (1 \leq j \leq 7, j \neq i) \qquad (S36)$$

$$\theta_{\mathrm{X}_j} \approx K_j^{-1} \theta_{\mathrm{X}_{j+1}}. \quad (1 \leq j \leq 7, j \neq i) \qquad (S37)$$

$$R_8 / \left(k_8 N_{\max_{\mathrm{all}}}\right) = \theta_{\mathrm{X}_8} - K_8^{-1} P_{\mathrm{CO_2}} \theta_{\mathrm{v_{all}}} \ll 1, \qquad (S38)$$

$$\theta_{\mathrm{X}_8} \approx \theta_{\mathrm{v_{all}}} P_{\mathrm{CO_2}} K_8^{-1}. \qquad (S39)$$

To describe θ_{X_j} using $\theta_{\mathrm{v_{all}}}$, θ_{X_j} is firstly expressed with θ_{X_1} or θ_{X_8} from the recurrence formula eqs. ($S36$) and ($S37$).

If j is smaller than i ($j \leq i$),

$$\theta_{\mathrm{X}_j} = K_{j-1} \theta_{\mathrm{X}_{j-1}} = K_{j-1} K_{j-2} \theta_{\mathrm{X}_{j-2}} = \cdots = \left(\prod_{f=1}^{j-1} K_f\right) \theta_{\mathrm{X}_1}. \qquad (S40)$$

If j is larger than i ($j > i$),

$$\theta_{\mathrm{X}_j} = K_j^{-1} \theta_{\mathrm{X}_{j+1}} = K_j^{-1} K_{j+1}^{-1} \theta_{\mathrm{X}_{j+2}} = \cdots = \left(\prod_{f=j}^{7} K_f^{-1}\right) \theta_{\mathrm{X}_8}. \qquad (S41)$$

Since θ_{X_1} and θ_{X_8} have already expressed by $\theta_{\mathrm{v_{all}}}$ (eqs. ($S34$) and ($S39$)), θ_{X_j} is expressed by $\theta_{\mathrm{v_{all}}}$ as

$$\theta_{\mathrm{X}_j} = \begin{cases} \theta_{\mathrm{v_{all}}} P_{\mathrm{CH_4}} \prod_{f=0}^{j-1} K_f & (j \leq i) \\ \theta_{\mathrm{v_{all}}} P_{\mathrm{CO_2}} \prod_{f=j}^{8} K_f^{-1} & (j > i) \end{cases}. \qquad (S42)$$

Since the total number of surface sites (sum of the vacant and filled sites) of the X_1–X_8 intermediate species is constant,

$$1 = \theta_{\mathrm{v_{all}}} + \theta_{\mathrm{X_1}} + \theta_{\mathrm{X_2}} + \cdots + \theta_{\mathrm{X}_i} + \cdots + \theta_{\mathrm{X_7}} + \theta_{\mathrm{X_8}}. \qquad (S43)$$

The following formula for θ_{X_j} is derived from eqs. (*S*42) and (*S*43).

$$\begin{aligned} 1 &= \theta_{\mathrm{v_{all}}} \left\{ \begin{matrix} 1 + P_{\mathrm{CH_4}}K_0 + P_{\mathrm{CH_4}}K_0K_1 + \cdots + P_{\mathrm{CH_4}}K_0K_1 \cdots K_i \\ + P_{\mathrm{CO_2}}K_{i+1}^{-1} \cdots K_8^{-1} + \cdots + P_{\mathrm{CO_2}}K_7^{-1}K_8^{-1} + P_{\mathrm{CO_2}}K_8^{-1} \end{matrix} \right\} \\ &= \theta_{\mathrm{v_{all}}} \left\{ 1 + P_{\mathrm{CH_4}} \sum_{l=1}^{i} \prod_{f=0}^{l-1} K_f + P_{\mathrm{CO_2}} \sum_{l=i+1}^{8} \prod_{f=l}^{8} K_f^{-1} \right\}, \end{aligned} \qquad (S44)$$

Therefore, $\theta_{\mathrm{v_{all}}}$ is derived as follows:

$$\theta_{\mathrm{v_{all}}} = \frac{1}{1 + P_{\mathrm{CH_4}} \sum_{l=1}^{i} \prod_{f=0}^{l-1} K_f + P_{\mathrm{CO_2}} \sum_{l=i+1}^{8} \prod_{f=l}^{8} K_f^{-1}}. \qquad (S45)$$

From eq. (*S*42), θ_{X_i} is also derived as follows:

$$\theta_{\mathrm{X}_i} = \frac{P_{\mathrm{CH_4}} \prod_{f=0}^{i-1} K_f}{1 + P_{\mathrm{CH_4}} \sum_{l=1}^{i} \prod_{f=0}^{l-1} K_f + P_{\mathrm{CO_2}} \sum_{l=i+1}^{8} \prod_{f=l}^{8} K_f^{-1}}. \qquad (S46)$$

Therefore, the $P_{\mathrm{CH_4}}$ profile of $R_{\mathrm{CO_2}}$ is derived as follows:

$$\begin{aligned} R_{\mathrm{CO_2}} &\approx k_i {N_{\mathrm{max_{all}}}}^2 \theta_{\mathrm{X}_i} \theta_{\mathrm{v_{all}}} \\ &= k_i {N_{\mathrm{max_{all}}}}^2 \left[\frac{P_{\mathrm{CH_4}} \prod_{f=0}^{i-1} K_f}{\left\{1 + P_{\mathrm{CH_4}} \sum_{l=1}^{i} \prod_{f=0}^{l-1} K_f + P_{\mathrm{CO_2}} \sum_{l=i+1}^{8} \prod_{f=l}^{8} K_f^{-1}\right\}^2} \right]. \end{aligned} \qquad (S47)$$

Under the experimental conditions, the inlet pressure of the methane gas was much higher than the pressure of the produced CO_2 gas ($P_{\mathrm{CH_4}} >> P_{\mathrm{CO_2}}$).[4] Therefore, assuming that $P_{\mathrm{CO_2}}$ in eq. (*S*47) is negligibly small compared with $P_{\mathrm{CH_4}}$, the $P_{\mathrm{CH_4}}$ dependence of $R_{\mathrm{CO_2}}$ and $R_{\mathrm{H_2}}$ can be expressed as

$$R_{\mathrm{CO_2}} \approx k_i {N_{\mathrm{max_{all}}}}^2 \left[\frac{P_{\mathrm{CH_4}} \prod_{f=0}^{i-1} K_f}{\left(1 + P_{\mathrm{CH_4}} \sum_{l=1}^{i} \prod_{f=0}^{l-1} K_f\right)^2} \right] = k_i' \left[\frac{K' P_{\mathrm{CH_4}}}{\left(1 + K' P_{\mathrm{CH_4}}\right)^2} \right], \qquad (S48)$$

$$K' \equiv \sum_{l=1}^{i} \prod_{f=0}^{l-1} K_f = K_0 + K_0K_1 + K_0K_1K_2 + \cdots + K_0K_1K_2 \cdots K_{i-1}, \qquad (S49)$$

$$k_i' \equiv \frac{k_i {N_{\mathrm{max_{all}}}}^2 \prod_{f=0}^{i-1} K_f}{\sum_{l=1}^{i} \prod_{f=0}^{l-1} K_f}. \qquad (S50)$$

Thus, even when the rate-determining step is not the forward reaction of $^{\bullet}CH_3$ (X_1) but rather another surface reaction involving different intermediate species ($X_i \rightarrow X_{i+1}$), the $P_{\mathrm{CH_4}}$ dependency similar to eq. (4) is derived.

S4. Discussion on the electron/hole transfer at metal/semiconductor interface

Our study indicates that some metal cocatalysts on semiconductor photocatalysts function as reduction sites by capturing electrons, while others act as oxidation sites by trapping holes.[2] Indeed, a recent transmission electron microscopy (TEM) observation conducted under non-illuminated and vacuum conditions revealed the coexistence of Pt metals capturing either electrons or holes on the same semiconductor (TiO_2) surface.[22] The authors of this paper attributed this phenomenon to variations in the work function of the contacted metals (ϕ_m), which arise from the coexistence of various metal crystal facets at the metal/semiconductor interface. These variations in ϕ_m influence the direction of charge transfer, thereby determining the direction of band bending (upward or downward) at the interface. Whether a loaded metal cocatalyst preferentially trap electrons or holes is governed by the relative difference in the work functions of the metal (ϕ_m) and the semiconductor (ϕ_s). On *n*-type semiconductor surfaces, such as Ga_2O_3 and TiO_2, electrons flow from the semiconductor to the metal when $\phi_m > \phi_s$, while holes transfer from the semiconductor to the metal when $\phi_m < \phi_s$.[23] Correspondingly, the energy bands of the *n*-type semiconductor bend upward toward the interface when $\phi_m > \phi_s$ and downward when $\phi_m < \phi_s$.[23]

Under light illumination conditions, the photogenerated electrons and holes separately migrate from the semiconductor to the metal cocatalysts along these downward and upward band bending regions, respectively, thereby suppressing charge recombination. Due to subtle structural difference in the loaded metal cocatalysts, such as variations in metal crystal facets at the interface, we consider that certain metal cocatalysts preferentially function as reduction sites by capturing electrons, while others act as oxidation sites by trapping holes.

S5. Kinetic analysis of P_{CH_4} profile of $R_{C_2H_6}$

As detailed in our previous study,[2] homocoupling of methyl radical intermediates ($2^{\bullet}CH_3 \rightarrow C_2H_6$) occurs on the surfaces for the Pt/Ga_2O_3 sample (Fig. S5-1a), while it proceeds in the gas phase for the Pd/Ga_2O_3 sample (Fig. S5-1b). Therefore, in the following two subsections (Supplementary Notes S5-1 and S5-2), we derive the P_{CH_4} profiles of the formation rate of C_2H_6 ($R_{C_2H_6}$) under two situations: (Case 1) homocoupling of methyl radical intermediates occurs on photocatalyst surfaces and (Case 2) homocoupling of methyl radical intermediates occurs in gas-phase, respectively.

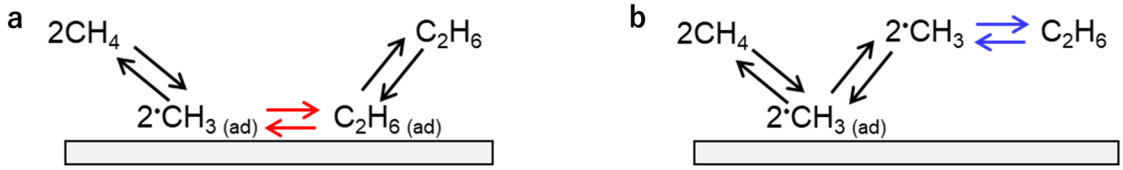

Fig. S5-1. Schematic kinetic model for ethane formation from methane through the coupling of photoactivated $^{\bullet}CH_3$ (**a**) on the surface and (**b**) in the gas phase.

S5-1. Case 1: Derivation of the P_{CH_4} profile of C_2H_6 formation rate under the situation where homocoupling ethane formation reaction is occurred on photocatalyst surfaces

First, we consider the case where the active sites for each intermediate species are independent and competition for reaction sites is negligible (Fig. S2-2). Based on our previous reports on the photocatalytic steam reforming of CH_4[2, 4] and discussion in the main text, the ethane formation process under the situation where homocoupling of methyl radical intermediates occurs on photocatalyst surfaces is described as follows:

$$\mathrm{CH_4}_{(gas)} + *_{\mathrm{v}} \underset{k_{de}}{\overset{k_{ad}}{\rightleftarrows}} {}^{\bullet}\mathrm{CH_3}_{(ad)}, \qquad (S51\_0)$$

$$2\,{}^{\bullet}\mathrm{CH_3}_{(ad)} + 2\,*_{\mathrm{v}'} \underset{k_{-1}}{\overset{k_1}{\rightleftarrows}} \mathrm{C_2H_6}_{(ad)} + 2\,*_{\mathrm{v}} + *_{\mathrm{v}'}, \qquad (S51\_1)$$

$$\mathrm{C_2H_6}_{(ad)} \underset{k_{-2}}{\overset{k_2}{\rightleftarrows}} \mathrm{C_2H_6}_{(gas)} + *_{\mathrm{v}'}. \qquad (S51\_2)$$

where $*_{\mathrm{v}}$ and $*_{\mathrm{v}'}$ denote vacant surface sites for methyl radicals and ethane, respectively. Eq. (S51_1) represents that two methyl radicals need to individually migrate from the adsorption sites to ethane formation surface sites for homocoupling reaction. The net reaction rates can be described as,

$$R_0 = k_{ad}P_{CH_4}N_{\mathrm{v}} - k_{de}N_{CH_3} = k_{ad}P_{CH_4}N_{max}\left(\theta_{\mathrm{v}} - K_0^{-1}P_{CH_4}^{-1}\theta_{CH_3}\right), \qquad (S52\_0)$$

$$\begin{aligned} R_1 &= k_1 N_{CH_3}^2 N_{\mathrm{v}'}^2 - k_{-1}N_{C_2H_6}N_{\mathrm{v}}^2 N_{\mathrm{v}'} \\ &= k_1 N_{max}^2 N_{max'}^2\left(\theta_{CH_3}^2\theta_{\mathrm{v}'}^2 - K_1^{-1}\theta_{C_2H_6}\theta_{\mathrm{v}}^2\theta_{\mathrm{v}'}\right), \end{aligned} \qquad (S52\_1)$$

$$R_2 = k_2 N_{C_2H_6} - k_{-2}P_{C_2H_6}N_{\mathrm{v}'} = k_2 N_{max'}\left(\theta_{C_2H_6} - K_2^{-1}P_{C_2H_6}\theta_{\mathrm{v}'}\right), \qquad (S52\_2)$$

where K_j denotes the equilibrium constant of the j-th reaction ($K_j \equiv k_j/k_{-j}$). N_{CH_3} and N_v are the number of filled and vacant surface sites for $^{\bullet}CH_3$ intermediate species, respectively. $N_{C_2H_6}$ and $N_{v'}$ are the number of filled and vacant surface sites for adsorbed C_2H_6 intermediate species, respectively. θ_{CH_3} ($\equiv N_{CH_3}/N_{max}$) and θ_v ($\equiv N_v/N_{max}$) are the coverage and the fraction of vacant surface sites for $^{\bullet}CH_3$ intermediate species, respectively. $\theta_{C_2H_6}$ ($\equiv N_{C_2H_6}/N_{max'}$) and $\theta_{v'}$ ($\equiv N_{v'}/N_{max'}$) are the coverage and the fraction of vacant surface sites for adsorbed C_2H_6 intermediate species, respectively. N_{max} and $N_{max'}$ are the sum of the numbers of filled and vacant surface sites for $^{\bullet}CH_3$ and C_2H_6 intermediate species, respectively ($N_{max} = N_{CH_3} + N_v \Leftrightarrow 1 = \theta_{CH_3} + \theta_v$, $N_{max'} = N_{C_2H_6} + N_{v'} \Leftrightarrow 1 = \theta_{C_2H_6} + \theta_{v'}$). Under steady-state conditions, the density of intermediate species is constant. As a result, the formation rate of C_2H_6 can be expressed as follows:

$$R_{C_2H_6} \equiv R_2 \approx R_1 \approx 0.5R_0. \qquad (S53)$$

In particular, when the coupling reaction (eq. (S51_1)) is rate-determining,[2, 4] the relation $\theta_{CH_3} >> \theta_{C_2H_6}$ is satisfied and the following equation is obtained from eqs. (S52_1) and (S53):

$$R_{C_2H_6} \approx R_1 \approx k_1 N_{max}^2 N_{max'}^2 \theta_{CH_3}^2 \theta_{v'}^2. \qquad (S54)$$

Defining the rate constant factor k_1'' as: $k_1'' \equiv k_1 N_{max}^2 N_{max'}^2$,

$$R_{C_2H_6} \approx k_1'' \theta_{CH_3}^2 \theta_{v'}^2. \qquad (S55)$$

As discussed in the Supplementary Note S2-1, θ_{CH_3} is expressed using Langmuir-adsorption-isotherm type equation (eq. (S10)) and most of the active sites for the reaction of $^{\bullet}CH_3$ species remain unoccupied ($\theta_{v'} \approx 1$) in the case where competitive occupation is negligible (Fig. S2-2). This is because the further homo-coupling reaction step ($2^{\bullet}CH_3 \rightarrow C_2H_6$) is rate-determining[2, 4] and the formed C_2H_6 species are immediately desorbed ($\theta_{C_2H_6} = 1 - \theta_{v'} \approx 0$). Therefore, the P_{CH_4} profile of $R_{C_2H_6}$ (Fig. S5-2) is derived from eq. (S55) as

$$R_{C_2H_6} \approx k_1'' \theta_{CH_3}^2 \approx k_1'' \left[\frac{(K_0 P_{CH_4})^2}{(1+K_0 P_{CH_4})^2}\right]. \qquad (S56)$$

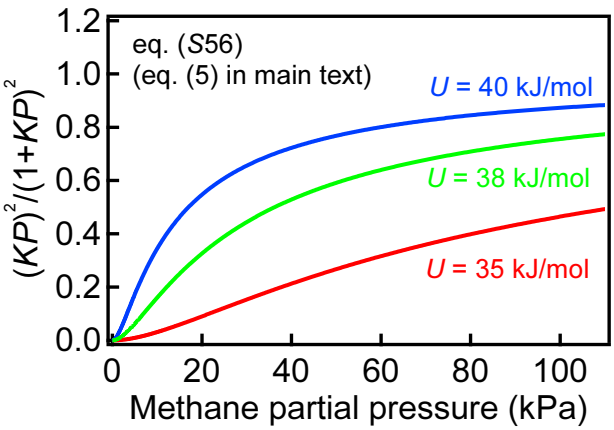

Fig. S5-2. P_{CH_4} dependence of $R_{C_2H_6}$ given by eq. (S56) at different values of U (35, 38, and 40 kJ/mol).

Then, we consider the case where density of surface reaction sites is low and the active sites are competitively shared among intermediate species (Fig. S2-3). The ethane formation process is described as follows:

$$\mathrm{CH_{4(gas)}} + *_{\mathrm{all}} \underset{k_{\mathrm{de}}}{\overset{k_{\mathrm{ad}}}{\rightleftarrows}} {}^{\bullet}\mathrm{CH_{3(ad)}}, \qquad (S57\_0)$$

$$2\ {}^{\bullet}\mathrm{CH_{3(ad)}} + 2\ *_{\mathrm{all}} \underset{k_{-1}}{\overset{k_1}{\rightleftarrows}} \mathrm{C_2H_{6(ad)}} + 3\ *_{\mathrm{all}}, \qquad (S57\_1)$$

$$\mathrm{C_2H_{6(ad)}} \underset{k_{-2}}{\overset{k_2}{\rightleftarrows}} \mathrm{C_2H_{6(gas)}} + *_{\mathrm{all}}. \qquad (S57\_2)$$

where $*_{\mathrm{all}}$ denotes the vacant surface active sites. Note that because the active sites are shared among the intermediate species, the vacant sites are described as $*_{\mathrm{all}}$ instead of $*_{\mathrm{v}}$ and $*_{\mathrm{v'}}$. Eq. (S57_1) represents that two methyl radicals need to individually migrate from the adsorption sites to vacant surface active sites for homocoupling reaction. The net reaction rates can be described as,

$$R_0 = k_{\mathrm{ad}} P_{\mathrm{CH_4}} N_{\mathrm{v_{all}}} - k_{\mathrm{de}} N_{\mathrm{CH_3}} = k_{\mathrm{ad}} P_{\mathrm{CH_4}} N_{\mathrm{max_{all}}} \left(\theta_{\mathrm{v_{all}}} - K_0^{-1} P_{\mathrm{CH_4}}^{-1} \theta_{\mathrm{CH_3}}\right), \qquad (S58\_0)$$

$$\begin{aligned} R_1 &= k_1 N_{\mathrm{CH_3}}^2 N_{\mathrm{v_{all}}}^2 - k_{-1} N_{\mathrm{C_2H_6}} N_{\mathrm{v_{all}}}^3 \\ &= k_1 N_{\mathrm{max_{all}}}^4 \left(\theta_{\mathrm{CH_3}}^2 \theta_{\mathrm{v_{all}}}^2 - K_1^{-1} \theta_{\mathrm{C_2H_6}} \theta_{\mathrm{v_{all}}}^3\right), \end{aligned} \qquad (S58\_1)$$

$$R_2 = k_2 N_{\mathrm{C_2H_6}} - k_{-2} P_{\mathrm{C_2H_6}} N_{\mathrm{v_{all}}} = k_2 N_{\mathrm{max_{all}}} \left(\theta_{\mathrm{C_2H_6}} - K_2^{-1} P_{\mathrm{C_2H_6}} \theta_{\mathrm{v_{all}}}\right), \qquad (S58\_2)$$

where $N_{\mathrm{v_{all}}}$ is the number of vacant surface sites. $\theta_{\mathrm{CH_3}}$ ($\equiv N_{\mathrm{CH_3}}/N_{\mathrm{max_{all}}}$) and $\theta_{\mathrm{C_2H_6}}$ ($\equiv N_{\mathrm{C_2H_6}}/N_{\mathrm{max_{all}}}$) are the coverage for adsorbed ${}^{\bullet}\mathrm{CH_3}$ and $\mathrm{C_2H_6}$ intermediate species, respectively. $\theta_{\mathrm{v_{all}}}$ ($\equiv N_{\mathrm{v_{all}}}/N_{\mathrm{max_{all}}}$) is the fraction of vacant surface sites. $N_{\mathrm{max_{all}}}$ is the sum of the numbers of filled and vacant surface sites ($N_{\mathrm{max_{all}}} = N_{\mathrm{CH_3}} + N_{\mathrm{C_2H_6}} + N_{\mathrm{v_{all}}} \Leftrightarrow 1 = \theta_{\mathrm{CH_3}} + \theta_{\mathrm{C_2H_6}} + \theta_{\mathrm{v_{all}}}$). Under steady-state conditions, the density of intermediate species is constant. As a result, the formation rate of $\mathrm{C_2H_6}$ can be expressed as follows:

$$R_{\mathrm{C_2H_6}} \equiv R_2 \approx R_1 \approx 0.5 R_0. \qquad (S59)$$

In particular, when the coupling reaction (eq. (S57_1)) is rate-determining,[2, 4] the relation $\theta_{\mathrm{CH_3}} >> \theta_{\mathrm{C_2H_6}}$ is satisfied and the following equation is obtained from eqs. (S58_1) and (S59):

$$R_{\mathrm{C_2H_6}} \approx R_1 \approx k_1 N_{\mathrm{max_{all}}}^4 \theta_{\mathrm{CH_3}}^2 \theta_{\mathrm{v_{all}}}^2. \qquad (S60)$$

Defining the rate constant factor k_1'' as: $k_1'' \equiv k_1 N_{\mathrm{max_{all}}}^4$,

$$R_{\mathrm{C_2H_6}} \approx k_1'' \theta_{\mathrm{CH_3}}^2 \theta_{\mathrm{v_{all}}}^2. \qquad (S61)$$

As discussed in the Supplementary Note S2-2, the coverage of intermediate species competitively affects the fraction of vacant surface sites in the case where competitive occupation is substantial (Fig. S2-3). Since the majority of the surface intermediates are ${}^{\bullet}\mathrm{CH_3}$ in case the reaction of adsorbed ${}^{\bullet}\mathrm{CH_3}$ intermediates is rate-determining,[2, 4] the fraction of vacant surface sites can be approximated as $\theta_{\mathrm{v_{all}}} \approx 1 - \theta_{\mathrm{CH_3}}$. Since $\theta_{\mathrm{CH_3}}$ is

expressed using Langmuir-adsorption-isotherm type equation (eq. (*S*25)), the P_{CH_4} profile of $R_{C_2H_6}$ (Fig. S5-3) is derived from eq. (*S*61) as

$$R_{C_2H_6} \approx k_1''\theta_{CH_3}^2\theta_{v_{all}}^2 \approx k_1''\theta_{CH_3}^2\left(1-\theta_{CH_3}\right)^2 \approx k_1''\left[\frac{\left(K_0P_{CH_4}\right)^2}{\left(1+K_0P_{CH_4}\right)^4}\right]. \qquad (S62)$$

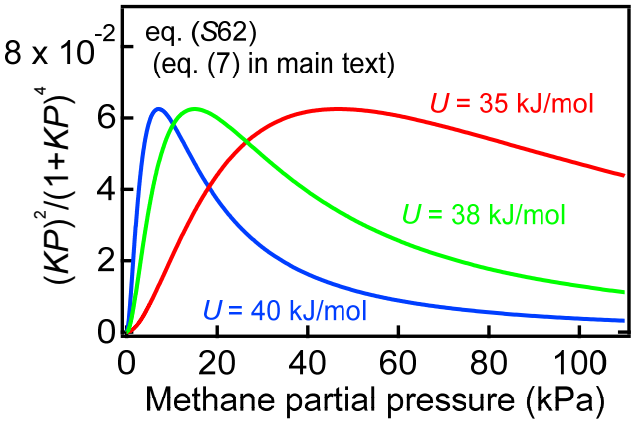

Fig. S5-3. P_{CH_4} dependence of $R_{C_2H_6}$ given by eq. (*S*62) at different values of *U* (35, 38, and 40 kJ/mol).

S5-2. Case 2: Derivation of the P_{CH_4} profile of C_2H_6 formation rate under the situation where homocoupling ethane formation reaction is occurred in gas-phase

In this subsection, we derive the P_{CH_4} dependence of the ethane formation rate in the case where ethane is produced by the homocoupling reaction of methyl radicals in the gas phase (Fig. S5-4).

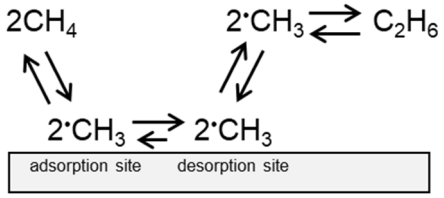

Fig. S5-4. Schematic kinetic model for ethane formation derived from the coupling reaction of gaseous methyl radicals.

First, we consider the case where the active sites for each intermediate species are independent and competition for reaction sites is negligible (Fig. S2-2). Based on our previous reports on the photocatalytic steam reforming of CH_4[2, 4] and discussion in the main text, the ethane formation process under the situation where homocoupling of methyl radical intermediates occurs in gas-phase is described as follows:

$$\mathrm{CH_{4(gas)}} + *_{\mathrm{v}} \underset{k_{\mathrm{de}}}{\overset{k_{\mathrm{ad}}}{\rightleftarrows}} {}^{\bullet}\mathrm{CH_{3(ad)}}, \qquad (S63\_0)$$

$${}^{\bullet}\mathrm{CH_{3(ad)}} + *_{\mathrm{v}'} \underset{k_{-1}}{\overset{k_1}{\rightleftarrows}} {}^{\bullet}\mathrm{CH_{3(ad)}}^{\star} + *_{\mathrm{v}}, \qquad (S63\_1)$$

$${}^{\bullet}\mathrm{CH_{3(ad)}}^{\star} \underset{k_{-2}}{\overset{k_2}{\rightleftarrows}} {}^{\bullet}\mathrm{CH_{3(gas)}} + *_{\mathrm{v}'}, \qquad (S63\_2)$$

$$2\ {}^{\bullet}\mathrm{CH_{3(gas)}} \underset{k_{-3}}{\overset{k_3}{\rightleftarrows}} \mathrm{C_2H_{6(gas)}}. \qquad (S63\_3)$$

Here, we consider the case where the adsorbed $^{\bullet}CH_3$ species are desorbed from surfaces after they migrate to other sites appropriate to desorption (Fig. S5-4). $*_v$ and $*_{v'}$ denote vacant surface sites for adsorption and desorption of methyl radicals, respectively and $^{\bullet}CH_3^{\star}$ represents the $^{\bullet}CH_3$ species on the desorption sites. The net reaction rates can be described as,

$$R_0 = k_{\mathrm{ad}} P_{\mathrm{CH_4}} N_{\mathrm{v}} - k_{\mathrm{de}} N_{\mathrm{CH_3}} = k_{\mathrm{ad}} P_{\mathrm{CH_4}} N_{\mathrm{max}} \left(\theta_{\mathrm{v}} - K_0^{-1} P_{\mathrm{CH_4}}^{-1} \theta_{\mathrm{CH_3}}\right), \qquad (S64\_0)$$

$$R_1 = k_1 N_{\mathrm{CH_3}} N_{\mathrm{v}'} - k_{-1} N_{\mathrm{CH_3}\star} N_{\mathrm{v}} = k_1 N_{\mathrm{max}} N_{\mathrm{max}'} \left(\theta_{\mathrm{CH_3}} \theta_{\mathrm{v}'} - K_1^{-1} \theta_{\mathrm{CH_3}\star} \theta_{\mathrm{v}}\right), \qquad (S64\_1)$$

$$R_2 = k_2 N_{\mathrm{CH_3}\star} - k_{-2} P_{\mathrm{CH_3}} N_{\mathrm{v}'} = k_2 N_{\mathrm{max}'} \left(\theta_{\mathrm{CH_3}\star} - K_2^{-1} P_{\mathrm{CH_3}} \theta_{\mathrm{v}'}\right), \qquad (S64\_2)$$

$$R_3 = k_3 P_{\mathrm{CH_3}}^2 - k_{-3} P_{\mathrm{C_2H_6}} = k_3 \left({P_{\mathrm{CH_3}}}^2 - K_3^{-1} P_{\mathrm{C_2H_6}}\right), \qquad (S64\_3)$$

where the population of $^{\bullet}CH_3$ species on the desorption sites and the number of vacant sites for desorption ($*_{v'}$) are denoted as $N_{CH_3\star}$ and $N_{v'}$, respectively. Their coverages are denoted as $\theta_{CH_3\star}$ ($\equiv N_{CH_3\star}/N_{max'}$) and $\theta_{v'}$ ($\equiv N_{v'}/N_{max'}$), where $N_{max'}$ is the total number of desorption sites for $^{\bullet}CH_3$ species ($N_{max'} = N_{CH_3\star} + N_{v'} \Leftrightarrow 1 = \theta_{CH_3\star} + \theta_{v'}$). Under steady-

state conditions, the density of intermediate species is constant. As a result, the formation rate of C_2H_6 can be expressed as follows:

$$R_{C_2H_6} \equiv R_3 \approx 0.5R_2 \approx 0.5R_1 \approx 0.5R_0. \qquad (S65)$$

In particular, when the migration from adsorption site to desorption site (eq. (*S*63_1)) is rate-determining, the relation $\theta_{CH_3} >> \theta_{CH_3\star}$ is satisfied and the following equation is obtained from eqs. (*S*64_1) and (*S*65):

$$R_{C_2H_6} \approx 0.5R_1 \approx 0.5k_1N_{max}N_{max'}\theta_{CH_3}\theta_{v'}. \qquad (S66)$$

Defining the rate constant factor k_1'' as: $k_1'' \equiv 0.5k_1N_{max}N_{max'}$,

$$R_{C_2H_6} \approx k_1''\theta_{CH_3}\theta_{v'}. \qquad (S67)$$

As discussed in the Supplementary Note S2-1, θ_{CH_3} is expressed using Langmuir-adsorption-isotherm type equation (eq. (*S*10)) and most of the active sites for the migration of $^{\bullet}CH_3$ species (eq. (*S*63_1)) remain unoccupied ($\theta_{v'} \approx 1$) in the case where competitive occupation is negligible (Fig. S2-2). This is because the further migration step ($^{\bullet}CH_3 \rightarrow {}^{\bullet}CH_3^{\star}$) is rate-determining and the formed $^{\bullet}CH_3^{\star}$ species are immediately desorbed ($\theta_{CH_3\star} = 1 - \theta_{v'} \approx 0$). Therefore, the P_{CH_4} profile of $R_{C_2H_6}$ (Fig. S5-5) is derived from eq. (*S*67) as

$$R_{C_2H_6} \approx k_1''\theta_{CH_3} \approx k_1''\left[\frac{K_0P_{CH_4}}{1+K_0P_{CH_4}}\right]. \qquad (S68)$$

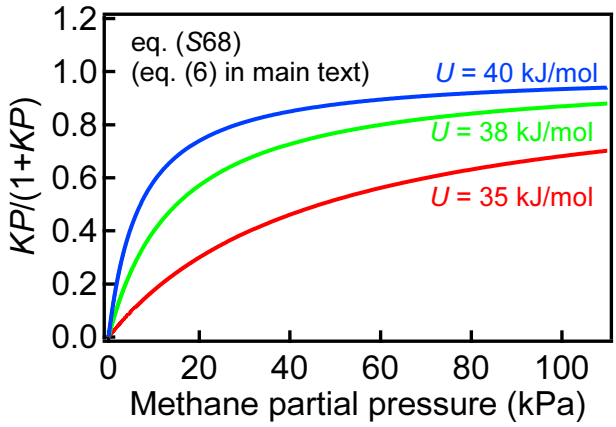

Fig. S5-5. P_{CH_4} dependence of $R_{C_2H_6}$ given by eq. (*S*68) at different values of U (35, 38, and 40 kJ/mol).

Then, we consider the case where density of surface reaction sites is low and the active sites are competitively shared among intermediate species (Fig. S2-3). The ethane formation process is described as follows:

$$\mathrm{CH_{4(gas)}} + *_{\mathrm{all}} \underset{k_{\mathrm{de}}}{\overset{k_{\mathrm{ad}}}{\rightleftarrows}} {}^{\bullet}\mathrm{CH_{3(ad)}}, \qquad (S69\_0)$$

$${}^{\bullet}\mathrm{CH_{3(ad)}} + *_{\mathrm{all}} \underset{k_{-1}}{\overset{k_1}{\rightleftarrows}} {}^{\bullet}\mathrm{CH_{3(ad)}}^{\star} + *_{\mathrm{all}}, \qquad (S69\_1)$$

$${}^{\bullet}\mathrm{CH_{3(ad)}}^{\star} \underset{k_{-2}}{\overset{k_2}{\rightleftarrows}} {}^{\bullet}\mathrm{CH_{3(gas)}} + *_{\mathrm{all}}, \qquad (S69\_2)$$

$$2\,{}^{\bullet}\mathrm{CH_{3(gas)}} \underset{k_{-3}}{\overset{k_3}{\rightleftarrows}} \mathrm{C_2H_{6(gas)}}, \qquad (S69\_3)$$

where $*_{\mathrm{all}}$ denotes the vacant surface active sites. Note that because the active sites are shared among the intermediate species, the vacant sites are described as $*_{\mathrm{all}}$ instead of $*_{\mathrm{v}}$ and $*_{\mathrm{v'}}$. The net reaction rates can be described as,

$$R_0 = k_{\mathrm{ad}} P_{\mathrm{CH_4}} N_{\mathrm{v_{all}}} - k_{\mathrm{de}} N_{\mathrm{CH_3}} = k_{\mathrm{ad}} P_{\mathrm{CH_4}} N_{\mathrm{max_{all}}} \left(\theta_{\mathrm{v_{all}}} - K_0^{-1} P_{\mathrm{CH_4}}^{-1} \theta_{\mathrm{CH_3}}\right), \qquad (S70\_0)$$

$$R_1 = k_1 N_{\mathrm{CH_3}} N_{\mathrm{v_{all}}} - k_{-1} N_{\mathrm{CH_3\star}} N_{\mathrm{v_{all}}} = k_1 N_{\mathrm{max_{all}}}^2 \left(\theta_{\mathrm{CH_3}} \theta_{\mathrm{v_{all}}} - K_1^{-1} \theta_{\mathrm{CH_3\star}} \theta_{\mathrm{v_{all}}}\right), \qquad (S70\_1)$$

$$R_2 = k_2 N_{\mathrm{CH_3\star}} - k_{-2} P_{\mathrm{CH_3}} N_{\mathrm{v_{all}}} = k_2 N_{\mathrm{max_{all}}} \left(\theta_{\mathrm{CH_3\star}} - K_2^{-1} P_{\mathrm{CH_3}} \theta_{\mathrm{v_{all}}}\right), \qquad (S70\_2)$$

$$R_3 = k_3 P_{\mathrm{CH_3}}^2 - k_{-3} P_{\mathrm{C_2H_6}} = k_3 \left({P_{\mathrm{CH_3}}}^2 - K_3^{-1} P_{\mathrm{C_2H_6}}\right), \qquad (S70\_3)$$

where $\theta_{\mathrm{CH_3\star}}$ ($\equiv N_{\mathrm{CH_3\star}}/N_{\mathrm{max_{all}}}$) is the coverage for ${}^{\bullet}\mathrm{CH_3}$ species on the desorption sites, and $N_{\mathrm{max_{all}}}$ is the sum of the numbers of filled and vacant surface sites ($N_{\mathrm{max_{all}}} = N_{\mathrm{CH_3}} + N_{\mathrm{CH_3\star}} + N_{\mathrm{v_{all}}} \Leftrightarrow 1 = \theta_{\mathrm{CH_3}} + \theta_{\mathrm{CH_3\star}} + \theta_{\mathrm{v_{all}}}$). Under steady-state conditions, the density of intermediate species is constant. As a result, the formation rate of C_2H_6 can be expressed as follows:

$$R_{\mathrm{C_2H_6}} \equiv R_3 \approx 0.5R_2 \approx 0.5R_1 \approx 0.5R_0. \qquad (S71)$$

In particular, when the migration from adsorption site to desorption site (eq. (S69_1)) is rate-determining, the relation $\theta_{\mathrm{CH_3}} >> \theta_{\mathrm{CH_3\star}}$ is satisfied and the following equation is obtained from eqs. (S70_1) and (S71):

$$R_{\mathrm{C_2H_6}} \approx 0.5R_1 \approx 0.5k_1 N_{\mathrm{max_{all}}}^2 \theta_{\mathrm{CH_3}} \theta_{\mathrm{v_{all}}}. \qquad (S72)$$

Defining the rate constant factor k_1'' as: $k_1'' \equiv 0.5k_1 N_{\mathrm{max_{all}}}^2$,

$$R_{\mathrm{C_2H_6}} \approx k_1'' \theta_{\mathrm{CH_3}} \theta_{\mathrm{v_{all}}}. \qquad (S73)$$

As discussed in the Supplementary Note S2-2, the coverage of intermediate species competitively affects the fraction of vacant surface sites in the case where competitive occupation is substantial (Fig. S2-3). Since the majority of the surface intermediates are ${}^{\bullet}\mathrm{CH_3}$ in case the migration of adsorbed ${}^{\bullet}\mathrm{CH_3}$ intermediates is rate-determining, the fraction of vacant surface sites can be approximated as $\theta_{\mathrm{v_{all}}} \approx 1 - \theta_{\mathrm{CH_3}}$. Since $\theta_{\mathrm{CH_3}}$ is expressed using Langmuir-adsorption-isotherm type equation (eq. (S25)), the $P_{\mathrm{CH_4}}$ profile of $R_{\mathrm{C_2H_6}}$ (Fig. S5-6) is derived from eq. (S73) as

$$R_{C_2H_6} \approx k_1''\theta_{CH_3}\theta_{v_{all}} \approx k_1''\theta_{CH_3}(1-\theta_{CH_3}) \approx k_1''\left[\frac{K_0P_{CH_4}}{(1+K_0P_{CH_4})^2}\right]. \quad (S74)$$

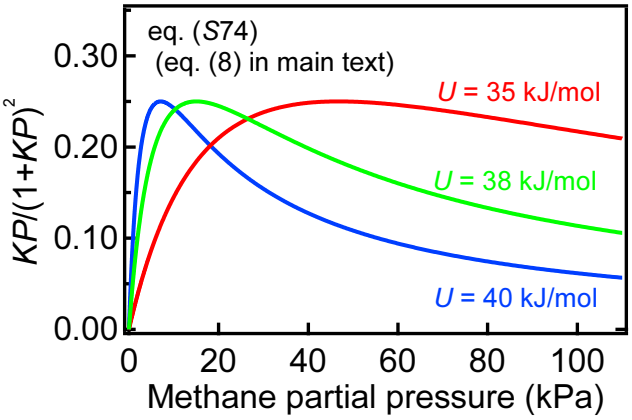

Fig. S5-6. P_{CH_4} dependence of $R_{C_2H_6}$ given by eq. (*S*74) at different values of U (35, 38, and 40 kJ/mol).

As described above and in the main text, $R_{C_2H_6}$ under steady-state condition is primarily determined by the rate-determining forward reaction of $^{\bullet}CH_3$ species as $R_{C_2H_6} \propto (\theta_{CH_3}\theta_v)^n$. When the density of surface reaction sites is sufficiently high, most active sites remain unoccupied, leading to $\theta_v \approx 1$. Conversely, when the density of surface reaction sites is not sufficiently high, the coverage of intermediate species competitively affects the fraction of vacant surface sites ($\theta_v \neq 1$). Therefore, the following four P_{CH_4} profiles of R_{C2H6} are derived: $R_{C_2H_6} \propto \theta_{CH_3}{}^2$ ($n = 2$ and $\theta_v \approx 1$; eq (*S*56) corresponding to eq (5) in the main text), $R_{C_2H_6} \propto \theta_{CH_3}$ ($n = 1$ and $\theta_v \approx 1$; eq (*S*68) corresponding to eq (6) in the main text), $R_{C_2H_6} \propto (\theta_{CH_3}\theta_v)^2$ ($n = 2$ and $\theta_v \neq 1$; eq (*S*62) corresponding to eq (7) in the main text), and $R_{C_2H_6} \propto \theta_{CH_3}\theta_v$ ($n = 1$ and $\theta_v \neq 1$; eq (*S*74) corresponding to eq (8) in the main text).

Fig. S5-7 shows the P_{CH_4} profiles of $R_{C_2H_6}$ given by these equations. As shown in Fig. S5-7a, $R_{C_2H_6}$ given by eq. (6) ($R_{C_2H_6} \propto \theta_{CH_3}$) exhibits an upward convex increase followed by saturation, whereas $R_{C_2H_6}$ given by eq. (5) ($R_{C_2H_6} \propto \theta_{CH_3}{}^2$) increases sigmoidally with P_{CH_4}. Therefore, based on the increasing trend of the experimentally observed $R_{C_2H_6}$, it is possible to deduce whether the homocoupling ethane formation reaction occurs on the photocatalyst surfaces ($n = 2$) or in the gas-phase ($n = 1$) in case where competitive site occupation is negligible ($\theta_v \approx 1$).

When competitive site occupation is substantial ($\theta_v \neq 1$), two opposing effects emerge: (i) the positive effect of increasing $^{\bullet}CH_3$ species concentration and (ii) the negative effect of molecular congestion due to the reduced availability of vacant active sites for further reactions, as shown in Fig. S5-7b. Notably, the decline of $R_{C_2H_6}$ is more significant for eq. (7) ($n = 2$; $R_{C_2H_6} \propto (\theta_{CH_3}\theta_v)^2$) than eq. (8) ($n = 1$; $R_{C_2H_6} \propto \theta_{CH_3}\theta_v$) (Fig. S5-7b). Therefore, by analyzing the decreasing behavior of the experimentally observed

$R_{C_2H_6}$, we can infer whether the homocoupling ethane formation occurs on the photocatalyst surfaces (n = 2) or in the gas-phase (n = 1).

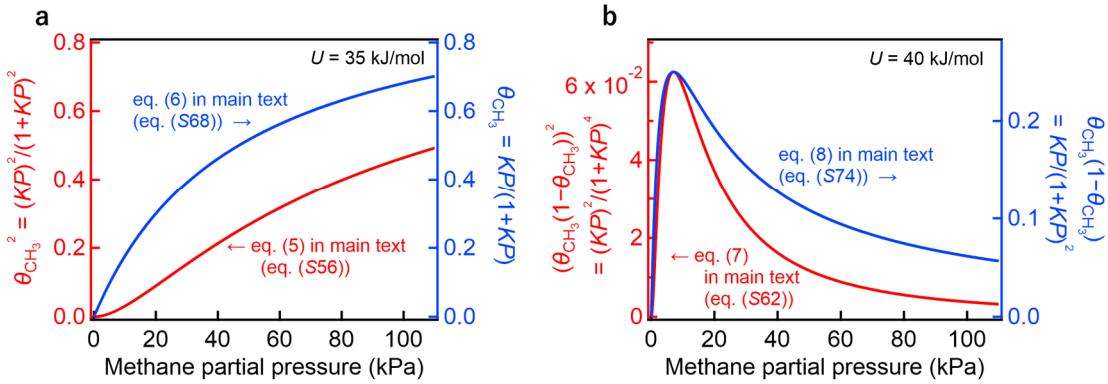

Fig. S5-7. (**a**) P_{CH_4} profiles of $R_{C_2H_6}$ given by eqs. (*S*56) and (*S*68) (corresponding to eqs. (5) and (6) in the main text) at U = 35 kJ/mol and (**b**) those given by eqs. (*S*62) and (*S*74) (corresponding to eqs. (7) and (8) in the main text) at U = 40 kJ/mol.

Based on these characteristic trends, we compared the fitting results of $R_{C_2H_6}$ using different equations, as shown in Fig. S5-8. For Pt(1wt%)/Ga_2O_3, which exhibits a sigmoidal increase at low P_{CH_4}, $R_{C_2H_6}$ was better fitted with eq. (5) ($R_{C_2H_6} \propto \theta_{CH_3}{}^2$), rather than eq. (6) ($R_{C_2H_6} \propto \theta_{CH_3}$) as shown in Fig. S5-8a. In contrast, for Pd(1wt%)/Ga_2O_3, which shows an upward convex increase, $R_{C_2H_6}$ was better fitted by eq. (6) than eq. (5) (Fig. S5-8b). These differences in the apparent reaction order suggest that the coupling of $^{\bullet}CH_3$ intermediates ($2^{\bullet}CH_3 \rightarrow C_2H_6$) occurs on the catalyst surfaces for the Pt(1wt%)/Ga_2O_3 sample, while it predominantly proceeds in the gas phase for the Pd(1wt%)/Ga_2O_3 sample. Similarly, for Pt(0.01wt%)/Ga_2O_3, which exhibits a steep decrease at high P_{CH_4}, $R_{C_2H_6}$ was better fitted with eq. (7) ($R_{C_2H_6} \propto (\theta_{CH_3}\theta_v)^2$), rather than eq. (8) ($R_{C_2H_6} \propto \theta_{CH_3}\theta_v$) as shown in Fig. S5-8c. In contrast, for Pd(0.01wt%)/Ga_2O_3, which shows a more gradual decrease at high P_{CH_4}, $R_{C_2H_6}$ was better fitted by eq. (8) than eq. (7) (Fig. S5-8d). These consistent differences in the apparent reaction order for $\theta_{CH_3}\theta_v$ suggest that the coupling of $^{\bullet}CH_3$ intermediates occurs on the catalyst surfaces for the Pt/Ga_2O_3 sample, while it predominantly proceeds in the gas phase for the Pd/Ga_2O_3 sample, irrespective of the loading amount.

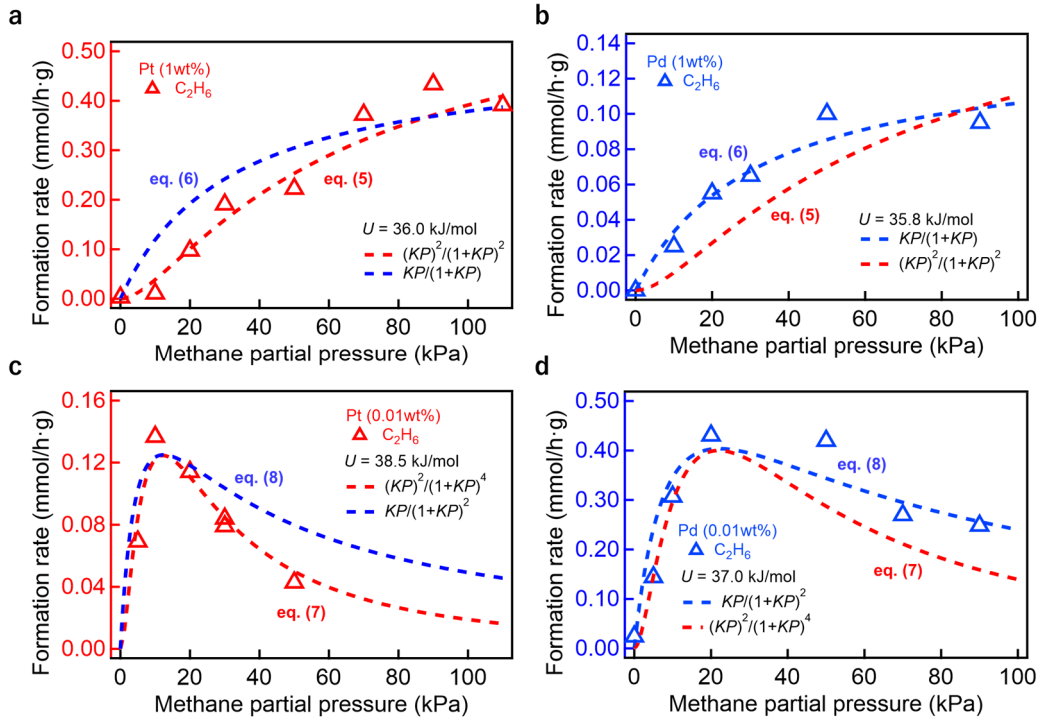

Fig. S5-8. P_{CH_4} profiles of photocatalytic ethane formation from methane and their fitting results. Formation rates of C_2H_6 for (**a**) Pt(1wt%)/Ga_2O_3, (**b**) Pd(1wt%)/Ga_2O_3, (**c**) Pt(0.01wt%)/Ga_2O_3, and (**d**) Pd(0.01wt%)/Ga_2O_3 photocatalysts under UV irradiation at P_{H_2O} = 2 kPa. Curve fitting results based on eqs. (5) and (6) with U = 36.0 kJ/mol, eqs. (5) and (6) with U = 35.8 kJ/mol, eqs. (7) and (8) with U = 38.5 kJ/mol, eqs. (7) and (8) with U = 37.0 kJ/mol are shown in (**a**), (**b**), (**c**), and (**d**), respectively.

Supplementary References

1. K. Shimura, T. Yoshida and H. Yoshida, *J. Phys. Chem. C*, 2010, **114**, 11466.
2. H. Saito, H. Sato, T. Higashi and T. Sugimoto, *Angew. Chem. Int. Ed.*, 2023, **62**, e202306058.
3. K. Shimura, K. Maeda and H. Yoshida, *J. Phys. Chem. C*, 2011, **115**, 9041.
4. H. Sato, A. Ishikawa, H. Saito, T. Higashi, K. Takeyasu and T. Sugimoto, *Commun. Chem.*, 2023, **6**, 8.
5. F. Amano, A. Ishikawa, H. Sato, C. Akamoto, S. P. Singh, S. Yamazoe and T. Sugimoto, *Catal. Today*, 2024, **426**, 114375.
6. S. Geller, *J. Chem. Phys.*, 1960, **33**, 676.
7. L. Yu, Y. Shao and D. Li, *Appl. Catal., B*, 2017, **204**, 216.

8. A. N. Pestryakov, V. V. Lunin, S. Fuentes, N. Bogdanchikova and A. Barrera, *Chem. Phys. Lett.*, 2003, **367**, 102.
9. H. A. Aleksandrov, K. M. Neyman, K. I. Hadjiivanov and G. N. Vayssilov, *Phys. Chem. Chem. Phys.*, 2016, **18**, 22108.
10. T. Avanesian, S. Dai, M. J. Kale, G. W. Graham, X. Pan and P. Christopher, *J. Am. Chem. Soc.*, 2017, **139**, 4551.
11. W. K. Kuhn, J. Szanyi and D. W. Goodman, *Surf. Sci.*, 1992, **274**, L611.
12. S. D. Ebbesen, B. L. Mojet and L. Lefferts, *Phys. Chem. Chem. Phys.*, 2009, **11**, 641.
13. L. Derita, S. Dai, K. Lopez-Zepeda, N. Pham, G. W. Graham, X. Pan and P. Christopher, *J. Am. Chem. Soc.*, 2017, **139**, 14150.
14. F. Zhang, L. Pan, T. Li, J. T. Diulus, A. Asthagiri and J. F. Weaver, *J. Phys. Chem. C*, 2014, **118**, 28647.
15. R. Lang, X. Du, Y. Huang, X. Jiang, Q. Zhang, Y. Guo, K. Liu, B. Qiao, A. Wang and T. Zhang, *Chem. Rev.*, 2020, **120**, 11986.
16. V. S. Bagotzky, Y. B. Vassiliev and O. A. Khazova, *J. Electroanal. Chem.*, 1977, **81**, 229.
17. G. Psofogiannakis, A. St-Amant and M. Ternan, *J. Phys. Chem. B*, 2006, **110**, 24593.
18. F. Amano, A. Shintani, K. Tsurui, H. Mukohara, T. Ohno and S. Takenaka, *ACS Energy Lett.*, 2019, **4**, 502.
19. D. A. Armstrong, R. E. Huie, W. H. Koppenol, S. V. Lymar, G. Merényi, P. Neta, B. Ruscic, D. M. Stanbury, S. Steenken and P. Wardman, *Pure Appl. Chem.*, 2015, **87**, 1139.
20. J. Nakamura, K. Kunimori and T. Uchijima, *Hyomen Kagaku*, 1991, **12**, 480.
21. H. Sato and T. Sugimoto, *J. Am. Chem. Soc.*, 2024, **146**, 24800.
22. R. Aso, H. Hojo, Y. Takahashi, T. Akashi, Y. Midoh, F. Ichihashi, H. Nakajima, T. Tamaoka, K. Yubuta, H. Nakanishi, H. Einaga, T. Tanigaki, H. Shinada and Y. Murakami, *Science*, 2022, **378**, 202.
23. Z. Zhang and J. T. Yates, *Chem. Rev.*, 2012, **112**, 5520.